processes

MDPI

Review

Pulsed Laser Deposition of Carbon-Based Materials: A Focused Review of Methods and Results

Rosalba Gaudiuso

Department of Chemistry, University of Bari "A. Moro", Via Orabona 4, 70126 Bari, Italy; rosalba.gaudiuso@uniba.it

Abstract: Pulsed Laser Deposition (PLD) is a highly flexible experimental methodology for the growth of thin films of a broad variety of materials, based on the generation of laser-induced plasmas (LIP) with material ablated from a solid target and on the transfer of the ablated material to a substrate. This review is focused on carbon-based materials—specifically, diamond-like carbon (DLC), graphene and carbyne—and will both discuss the influence of the most critical experimental parameters on the obtained materials and present the experimental developments proposed in the recent literature to tailor the properties of the deposited films and optimize the standard PLD technique for production of various carbon-based materials.

Keywords: pulsed laser deposition (PLD); diamond-like carbon (DLC); graphene; carbon-atom wire (CAW); carbyne

Citation: Gaudiuso, R. Pulsed Laser Deposition of Carbon-Based Materials: A Focused Review of Methods and Results. *Processes* **2023**, *11*, 2373. https://doi.org/10.3390/pr11082373

Academic Editor: Maura Cesaria

Received: 20 June 2023
Revised: 1 August 2023
Accepted: 2 August 2023
Published: 7 August 2023

1. Introduction

Italian writer and Holocaust survivor Primo Levi, a chemist by education and trade, closed his 1975 short story collection *The Periodic Table* with the tale of a carbon atom, from a very static existence as $CaCO_3$ in a rock ("Our character lies for hundreds of millions of years, bound to three atoms of oxygen and one of calcium, in the form of limestone") to an extremely active one as part of the nerve cells of the author himself in the act of writing the very short story *Carbon* ("It is that which at this instant, issuing out of a labyrinthine tangle of yeses and nos, makes my hand run along a certain path on the paper, mark it with these volutes that are signs: a double snap, up and down, between two levels of energy, guides this hand of mine to impress on the paper this dot, here, this one." [1]).

While the carbon atom journey described by Levi is clearly a literary device produced by the author's imagination, most science students and scholars are familiar with the central role of this element in both inorganic and organic chemistry. Carbon atoms can bind with each other with three possible hybridizations (i.e., sp, sp^2, sp^3) and the element can, therefore, exist in a variety of allotropes. Some of these have been long known, such as diamond and graphite, while others have been recently discovered, such as graphene and fullerene, and there are still others whose existence has not yet been unequivocally proven, i.e., carbyne. Carbon allotropes, their derivatives and their corresponding hybridizations are schematically reported in Figure 1.

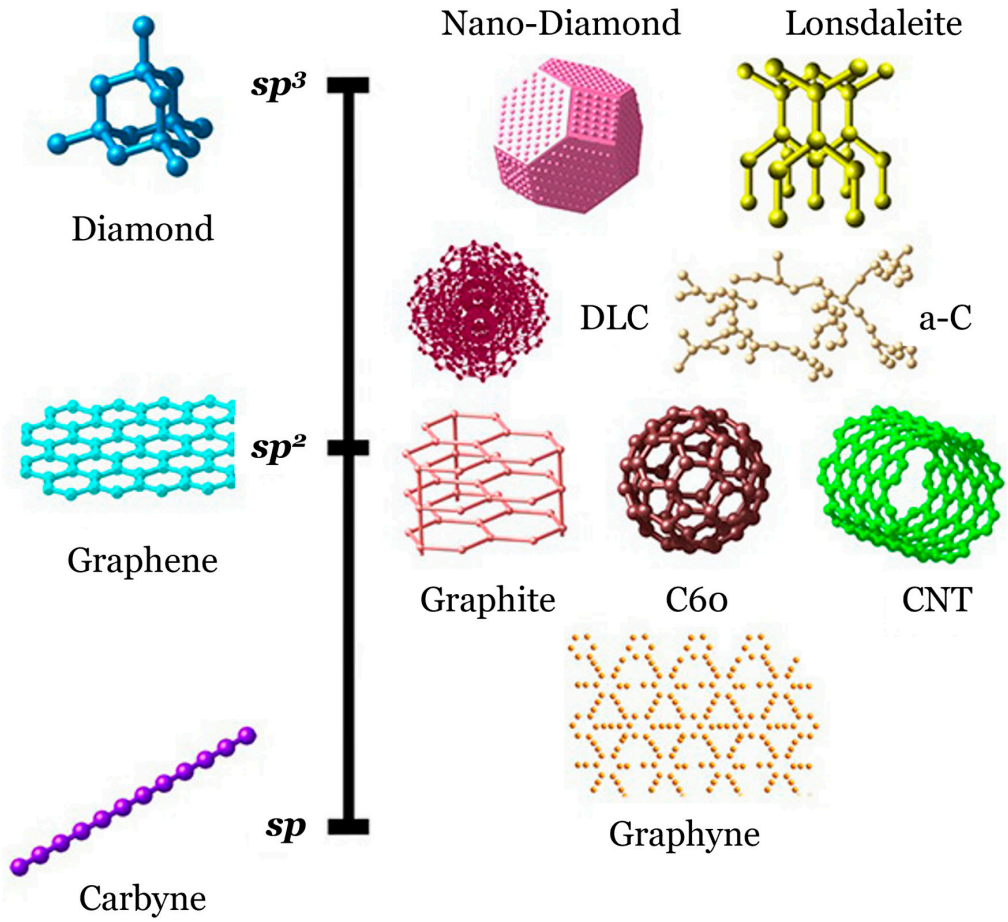

Figure 1. Carbon allotropes with their corresponding hybridizations and derivatives. Here, graphite is indicated as being derived from multiple stacked single-layer graphene sheets. Adapted with permission from [2]. Copyright 2022, Elsevier.

This great structural variety corresponds to an equally ample variety of mechanical, thermal, electrical and chemical properties of possible use in myriad fields of science and industry [3,4].

Therefore, many experimental techniques have been and are still being developed to produce C-based materials with controlled chemistry and morphology, aiming both to implement scalable methods for industry applications and to gain fundamental insight into currently less understood aspects of carbon chemistry. These include chemical methods, such as chemical synthesis [5–7], Chemical Vapor Deposition (CVD) [8–13], pyrolysis [14–16] and Atomic Layer Deposition (ALD) [17–20], and physical deposition methods, such as sputtering [17–20] and Molecular Beam Epitaxy (MBE) [21–23].

Laser-based techniques, including Pulsed Laser Deposition (PLD), have been emerging in the last two decades as some of the most efficient and versatile methods for the synthesis of thin films and nanoparticles of myriad materials, ranging from electronic and biocompatible ceramic materials, metals and composites, metal oxides and high-temperature superconductors (HTSCs) to the C-based materials of interest in this review [24–33] (and references therein).

Virtually any kind of carbon-based material has been deposited by PLD, ranging from amorphous carbon materials containing mixtures of carbon atoms with various hybridizations to predominantly sp^3-hybridized diamond-like carbon (DLC); sp^2-hybridized graphene, nanotubes, fullerenes and graphite; and sp-hybridized polyynes and carbon-atom wires [34–36].

These techniques are based on generating a laser-induced plasma (LIP) with an intense laser beam focused on the surface of a solid target of choice. During its expansion, the

ablated material can interact with the background environment and ultimately deposit as a thin film upon reaching a substrate.

Even from the simplified picture just provided, it is clear that intrinsic simplicity is the main advantage of laser ablation techniques. The use of a source of energy, the laser, that is external to the deposition chamber, and therefore independent of it, bestows exceptional experimental flexibility to this technique. First and foremost, background gases of different kinds, pressures and compositions can be used in the deposition chamber, thus enabling a whole range of tunable chemical interactions between the ablated species and the background gas itself. At the same time, various experimental arrangements are possible with the same apparatus, in terms of both deposition geometries and additional instrumental modules (such as support electrical discharges or magnetic fields).

Moreover, toxic precursors are not normally required, which makes PLD more environmentally friendly than techniques such as CVD and chemical synthesis, and its milder operating conditions can result in a lower-cost experimental apparatus, particularly when using nanosecond lasers.

On the other hand, PLD also has some important drawbacks, such as the high directionality of the plume, which can result in film inhomogeneity (in terms of chemistry, thickness and uneven substrate coverage) and the presence of particulates, which requires careful experimental optimization, especially for applications such as high-performance optics and electronics where stringent quality requirements of smoothness and defect density must be met.

This review will start by providing an overview of the fundamental processes underlying PLD (Section 2). It will then review experimental methods and results reported in the PLD literature (focusing especially on the period 2003–2023) for the generation of C-based materials with each possible hybridization, from sp^3 DLC (Section 3), to sp^2 graphene (Section 4) and sp carbyne (Section 5). It will then draw some conclusions on the state of the art and outline some possible future directions in this exciting field of research (Section 6).

2. Fundamental Concepts of PLD

In PLD, the laser beam is focused on a rotating or translating target placed inside a vacuum chamber, which also contains a substrate at a given distance from the target and is equipped with optical windows for laser access and optional online spectroscopic monitoring, a pressure gauge and a vacuum system consistent with the level of vacuum required by the chosen experimental conditions. Figure 2 schematically shows a typical experimental apparatus for PLD.

The PLD process can be thought of as divided into three different steps: material ejection upon target irradiation; plasma expansion; and deposition of ablated material on the substrate.

A detailed description of the first two steps (laser ablation and laser-induced plasma evolution) would be beyond the scope of this review, but a simplified overview is nonetheless provided below. Interested readers may find additional resources on laser-induced plasmas in [37–42].

The transfer of electromagnetic energy during the laser–matter interaction transfers energy to electrons in the target, which can result in the vaporization (i.e., ablation) of the irradiated portion of the target and the atomization, ionization and excitation of the ablated material. This series of events is referred to as laser-induced breakdown (LIB) and is a threshold phenomenon that can only occur if the power density of the laser (irradiance, usually measured in W/cm^2) exceeds the breakdown threshold of the material. Several phenomena can combine and contribute to the breakdown to extents that depend on the employed laser source (wavelength, pulse duration, irradiance) and on the irradiated material (state of aggregation, physical–chemical characteristics).

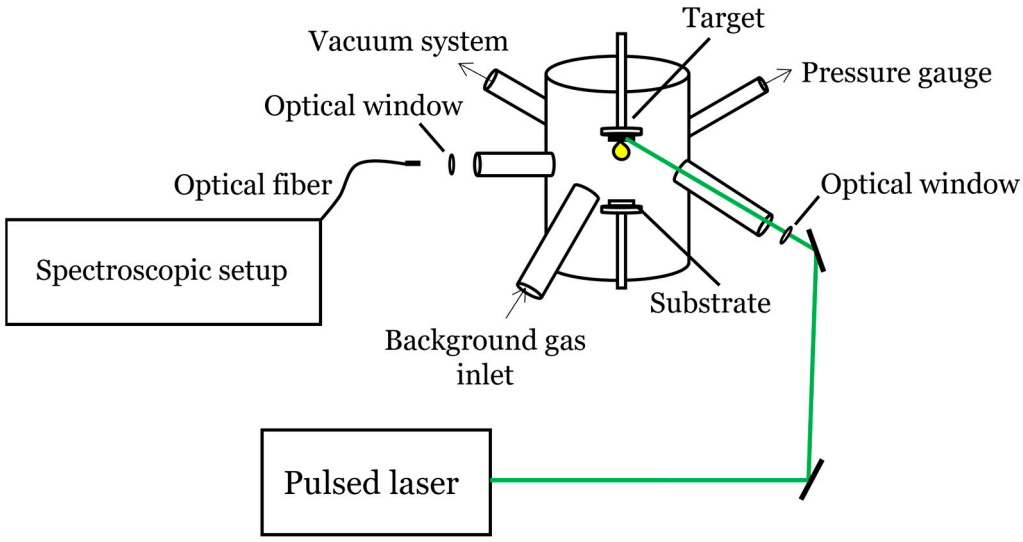

Figure 2. Schematics of a basic PLD experimental apparatus, comprising a pulsed laser source; a deposition chamber with optical access for the laser and optional online spectroscopic diagnostics; target and substrate holder; vacuum system; and pressure gauge.

Broadly speaking, the LIB tends to be dominated by thermal effects with lasers having long pulse amplitude (i.e., in the order of nanoseconds) and long wavelengths (i.e., IR), especially with metallic targets. The thermal character is more limited with short wavelengths (i.e., UV) and, even at long wavelengths, with short and ultrashort pulse amplitudes (i.e., in the order of picoseconds and nanoseconds). For the latter, the ablation is mostly electrostatic because the timescale of electron–phonon collisions is longer than the duration of the laser pulse itself (two-temperature ablation model), which causes fast ejection of electrons and subsequent ablation of the positively charged lattice (Coulomb explosion).

Once ablated, the material expands at supersonic speed, in a direction roughly orthogonal to the target, and de-excites, mostly by electron impact but also emitting radiation. In the case of nanosecond pulses, the tail of the laser pulse can interact with the already-formed plasma and transfer further energy to the ablated material through inverse bremsstrahlung.

The radiation emitted by the expanding plasma can be detected and used for online process diagnostics and determination of fundamental plasma parameters, such as temperature and electron density. The optical emission spectroscopy of LIPs is referred to as Laser-Induced Breakdown Spectroscopy, or LIBS (or, less frequently, LIPS, Laser-Induced Plasma Spectroscopy [43–50] (and references therein)).

The persistence time of the LIP plume depends on the laser source (with ns-LIPs lasting longer than ps- and fs-LIPs) and on the background environment where it has been generated, which can be a gas at atmospheric, reduced or high pressure; vacuum; or a liquid [51,52]. During its evolution, the LIP can physically and chemically interact with the background environment and can thus produce materials with the same or different chemistry than the target from which they have been generated [28–30]. In the case of a gaseous background, these materials can deposit as thin films on a substrate positioned at a given distance from the target, and the technique is referred to as PLD. In the case of a liquid environment, they can form a colloidal dispersion of nanoparticles, and the technique is referred to as Pulsed Laser Ablation in Liquids (PLAL).

While carbon-based materials can be and have been successfully synthesized by PLAL [53–57], this review will not address this technique in detail and will instead focus exclusively on PLD, specifically for the deposition of carbon-based thin films. Interested readers are referred to several review and perspective papers that have appeared in the recent PLAL literature for details on this experimental method [58–60].

To complete this introduction to PLD, a brief mention is given here to the main issues correlated to the actual deposition of ablated particles on the substrate surface and the experimental strategies to improve the film quality.

The production of particulates is an intrinsic problem in PLD, and its occurrence can be affected by many experimental parameters, such as laser fluence and wavelength, background gas pressure and substrate-to-target distance, as well as by the chemical nature of the irradiated target [28–30].

Particulates generated during PLD can be of three different kinds, each arising from a different phenomenon: (1) solid particles of irregular shape and micro- to nano-sized dimensions, which can be formed by the detachment of target fragments due to laser-induced mechanical and thermal shock, especially in the presence of surface irregularities such as cracks and pits, or even by the sudden escape of gas bubbles trapped in the target; (2) liquid droplets of micron and submicron dimensions, which can originate from the ejection of molten material from subsurface superheated layers and the recoil pressure of the just-formed plasma on the molten pool, especially when the ablation event is very fast; (3) nano-sized particles, produced by condensation and chemical reactions of plasma species with background gas species, particularly at high background pressures.

While a disadvantage when depositing films with the same composition as the target, the formation of this third kind of particulate can be a useful tool to synthesize materials with different chemistry and can thus be tailored accordingly by acting on pressure and composition of the background gas (reactive PLD) [28,29].

The amount of solid particulate can be minimized by using targets with smooth and polished surfaces, and non-porous materials with high and constant density.

Liquid droplets depend in a complex way on the process parameters, and though the high heterogeneity of materials that can be irradiated for PLD purposes make any generalization difficult and scarcely significant, some guidelines can nonetheless be provided, particularly concerning the influence of laser wavelength, fluence and background gas pressure [30]. First, the smaller the absorption coefficient, the longer the laser penetration depth, and the higher the particulate density and dimensions; therefore, when irradiating materials with an inverse proportionality between absorption coefficient and laser wavelength, films deposited with longer wavelengths are expected to contain more particulates than those deposited with shorter wavelengths.

Clearly, since laser ablation with different wavelengths and pulse durations occurs with different mechanisms, such behavior cannot be generalized a priori but should be verified on a case-by-case basis.

As for fluence, all materials show a certain threshold value which, when exceeded, can cause ejection of droplets to increase rapidly. The threshold value is strongly dependent on materials and lasers, and the particulate dimensions do not necessarily follow a monotonic trend with fluence.

Finally, for what concerns the background gas influence, increasing pressure usually increases the particulate dimensions, because the residence time of ejected droplets in the gas phase increases, and so does the probability that they will undergo collisions, acquire material and grow in dimensions. For the same reason, placing the substrate at a longer distance from the target can promote the formation and deposition of larger droplets on the substrate.

Two main approaches are possible to reduce the particulate and can be also combined to obtain better results [28–30]: (i) destroying the particulate or preventing it from reaching the substrate; (ii) acting on experimental parameters to limit the formation of particulate.

The first approach can be implemented with mechanical devices, such as a mechanical velocity filter between the target and the substrate to stop heavy and slower particles, or with geometrical deposition strategies such as off-axis growth. Since the flow of heavy particles is more sharply directed (perpendicular to the target surface) than that of light ones, placing the substrate either at a distance from the plasma axis (Figure 3b) or at an angle from the target (Figure 3c), can improve the film quality, though reducing the deposition rate.

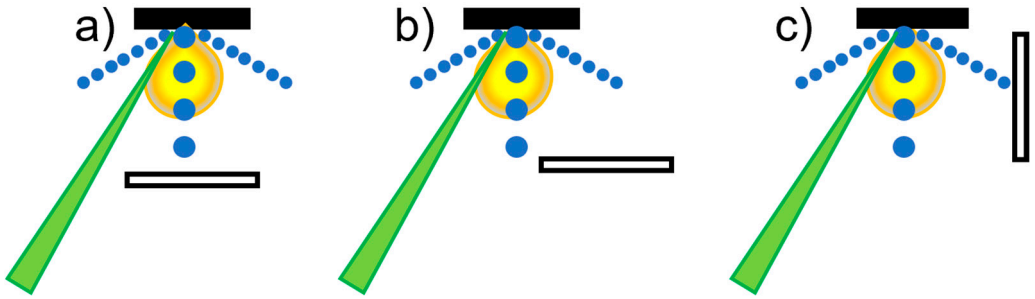

Figure 3. (**a**–**c**). Schematic representation of three possible PLD geometries: line of sight geometry, in which the substrate can face the substrate either (**a**) on-axis or (**b**) off-axis; (**c**) non-line-of-sight geometry, in which the substrate is at an angle with respect to the target (usually orthogonal). The incoming laser beam generating the plasma is represented as a green wedge impinging on the target from the bottom left. The different directions of the flux of large and small particulates are also schematically shown in the picture, with heavier particles traveling orthogonal to the target and the lighter ones traveling at a smaller angle and describing a funnel shape. Line-of-sight off-axis and non-line-of-sight geometries can be chosen to limit the amount of heavy particulate reaching the substrate and, therefore, to reduce their incorporation into the growing film.

Another approach involves the use of an additional source of energy, such as a second laser pulse, parallel to the target surface and suitably delayed with respect to the ablation laser, to destroy the particulates in the plasma before they can reach the target. Instead of a second laser pulse, a DC or RF discharge can be used to generate an additional plasma between the target and substrate, thus also acting as a substrate activator and enhancing ion bombardment thanks to the imposed negative bias [61,62].

3. PLD of Diamond-like Carbon

Diamond-like carbon (DLC) indicates a carbon thin film consisting of an amorphous or crystalline mixture of carbon atoms with predominantly sp^2 and sp^3 hybridization, in variable proportions, which can also contain sp-hybridized carbon atoms and hydrogen.

The higher the sp^3-C percentage and the lower the hydrogen amount, the more similar DLC is to natural diamond, and it can therefore show some of its remarkable properties. The latter are summarized in Table 1, together with the related potential applications of DLC films.

Table 1. Mechanical, thermal and optical properties of natural diamond and related potential applications of DLC [35,63,64] (and references therein).

Properties of Natural Diamond	Applications of DLC Films
Mechanical hardness (~90 GPa) Highest known bulk modulus (1.2×10^{12} N/m^2) Lowest known compressibility (8.3×10^{-13} m^2/N)	• Protective and hardening coatings for cutting tools • Wear-resistant and tribological coatings
Highest known thermal conductivity at room temperature (2×10^3 W m^{-1} K^{-1})	• Heat sink for laser diodes and integrated circuits
Optical transparency from deep UV to far IR	• Protective coatings for optical elements in harsh environments • Detectors for ionizing radiations (VUV and X-ray)
Good electrical insulator (resistivity at room temperature ~10^{16} Ω cm) Possibility of doping to obtain wide band-gap semiconductor (5.4 eV)	• Use in electronic devices as insulator or, if doped, as high band-gap semiconductor
High chemical inertness and resistance to corrosion	• Coatings and electrodes with high resistance to chemical attacks • Coatings for medical instruments, implants and prostheses • Biosensors
Biological compatibility (high inertness, low friction)	

Research efforts for DLC film production, therefore, have been primarily aimed at developing strategies to maximize the sp^3 fraction and minimize the incorporation of hydrogen into the film. In PLD, this can be achieved by acting on the three main experimental parameters which, as mentioned in Section 1, can crucially affect the PLD process, i.e., laser source; kind and pressure of background gas; and substrate.

Accurately optimizing these parameters can enable making the most of the specific advantages that this technique can offer with respect to other well-established thin-film deposition technologies, such as CVD and magnetron sputtering. These advantages include milder and safer deposition conditions due to the absence of gaseous precursors, as well as lower substrate temperature, which makes the technique more environmentally friendly and better suited for depositions on delicate substrates (e.g., polymers [65,66], glass [67]); the generation of carbon species with kinetic energies suited for the maximization of an sp^3-hybridized carbon atom fraction (discussed in the following); and the possibility of growing hydrogen-free films, which can be desirable since hydrogenated DLC films feature worse mechanical, optical and thermal properties than nonhydrogenated ones [31,68] (and references therein).

Since graphite is the thermodynamically stable allotrope of carbon, the most common targets used for PLD of DLC films are sintered, pyrolytic or glassy graphite, and the whole process of laser ablation, plasma production and deposition of the ablated species is meant to produce an $sp^2 \rightarrow sp^3$ transition.

To do this, the C plasma species must reach the target, where they will start to nucleate to form the DLC film, with an optimal kinetic energy value of around 100 eV [64]). This energy, according to the so-called ion subplantation model, can promote the formation of layers which contain the kinetically favored allotropic form of C, i.e., the sp^3-hybridized diamond. Incident particles with enough kinetic energy can reach deeper layers of the growing film, thus occupying subsurface positions and enabling the formation of sp^3 films thicker than a few monolayers. On the other hand, C species with lower kinetic energy cannot penetrate the outer film layers and remain on the surface. In this condition, the thermodynamically favored sp^2-hybridized graphite forms. Nonetheless, kinetic energy values that are both higher and lower than the optimal one can be detrimental to the quality of the forming film. If the C species have much higher kinetic energy, the ensuing ionic bombardment can be too energetic, which can cause the growing film to be mechanically and thermally damaged, exfoliated and, eventually, even desorbed.

This parameter should therefore be carefully controlled, which can be done by acting on several experimental variables: laser source; additional energy sources; background gas; target characteristics; and distance from the substrate. The effect played by each of these variables and their consequences on the quality of the obtained DLC films are described in the following section.

The focus of the following overview is on the diamond character since this is ultimately the most important parameter of DLC films. Nonetheless, other important features include crystallinity, substrate adhesion and homogeneity (in terms of thickness and particulate density). Several of the experimental strategies that will be described in the following, and that were meant to maximize the diamond character, have also been used to improve these aspects. For example, accelerating C species and improving ion bombardment can reduce the residual stress of the growing films, thus improving their adhesion to substrates, while using additional sources of energy, such as double laser pulses or magnetic fields, can reduce the amount of particulates and clusters reaching the substrate, thus improving the film homogeneity [35] (and references therein).

3.1. Laser Wavelength, Fluence and Pulse Width

Figure 4, from the excellent review by Lu et al. [35], summarizes the most salient results from the literature about the combined effect of laser wavelength and fluence on the percentage of sp^3 bonds. Generally speaking, the diamond character tends to increase with decreasing wavelength and with increasing fluence, with the best results provided

by excimer lasers (ArF 193 nm and, especially, KrF lasers, both having pulse duration around 20–25 ns) and the worst provided by IR lasers (Nd:YAG 1064 nm, 7 ns). This can be justified by the fact that UV lasers have higher photon frequencies; thus, they are better suited to cleave chemical bonds in non-metals and produce carbon plasmas with a higher ionization degree, while at the same time limiting thermal ablation effects, which are typical of longer ablation wavelengths, such as the formation of clusters and melted graphite droplets [31–35] (and references therein).

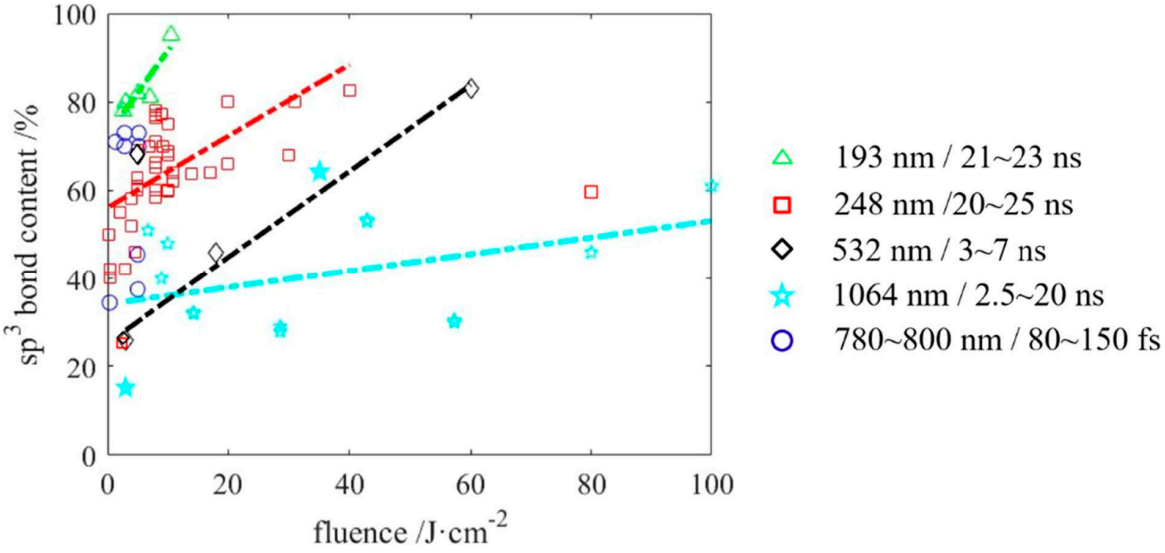

Figure 4. Variation of the percentage of sp^3-hybridized C atoms in DLC films as a function of laser fluence for laser sources of different wavelength and pulse amplitude. Reproduced with permission from [35]. Copyright 2021, Elsevier.

Nonetheless, while a high sp^3 percentage is generally desirable, an increase in this feature has also been observed to cause internal stress and poor substrate adhesion, especially in films grown at high fluence. This suggests that, when working with pulse widths in the order of nanoseconds, the best choice is using relatively low fluence and short wavelength.

Moreover, while thermal ablation effects can also be minimized with ultrashort lasers (see Section 1), this does not necessarily translate into a higher sp^3 fraction, as displayed in Figure 4. Here, ultrashort lasers (780–800 nm, 80–150 fs) are shown to provide higher sp^3 content than longer pulses at the same low fluences, but this percentage does not exceed 80%, thus causing ultrashort lasers to be outperformed by UV and visible nanosecond lasers at relatively higher fluence. This is a direct consequence of the differences between the LIP formation and evolution with long and ultrashort pulse widths, particularly the lack of inverse bremsstrahlung and comparably less efficient ionization and translational excitation in the case of femtosecond laser pulses and the larger amount of molecular radicals directly ensuing from the target. Ultrashort lasers are, therefore, not the most usual choice for PLD of DLC.

In addition to the pulse amplitude, the size and shape of the laser beam are other factors that can have an important impact on the quality of the deposited films. With tightly focused laser beams, the LIP expansion tends to resemble a point explosion, and is therefore accompanied by a larger angular spread of the ablated species, while less focused beams produce more forward-expanding LIPs. Consequently, more homogeneous films can be grown with less focused beams since the ablation plume is tighter in this case. This is also reflected in the fact that the shape of the beam's cross section can affect the plasma shape, expansion dynamics and geometry and, ultimately, alter the homogeneity and quality of the growing films. Excimer lasers, which are currently the laser source of choice for PLD of DLC, have rectangular cross sections. Therefore, plasmas generated by such lasers can have an anisotropic expansion along the short and long axis of the

rectangle (flip-over effect), thus affecting the sp^3 fraction and growth rate of the DLC films in turn [31]. Moreover, the occurrence of a peculiar V-shape in plasmas produced with excimer lasers has been recently observed by Ursu et al. [69] and Cesaria et al. [68]. These works, which described the formation of two lobes expanding at an angle from each other and recombining into a single plume at later stages of the plasma evolution, indicate how an accurate study of plasma dynamics and spatially resolved composition in the presence of such unconventional expansion behavior could be key to significantly improving the chemical and morphological quality of the deposited films.

3.2. Additional Sources of Energy

As discussed previously, carbon species are required to have an optimal kinetic energy (100 eV) to maximize the sp^3-C fraction, both to enable ion subplantation and to diffuse across and underneath the film surface. Besides acting on the laser source, as described in the previous section, various other strategies have been tested to provide the required energy.

The first of these approaches is activating the surface by inducing energetic ion bombardment, which can be done in two main ways: (i) accelerating the plasma ions by adding a negative bias to the substrate, which is effective with IR laser sources, but not with the more commonly used UV laser sources [70,71]; (ii) assisting the deposition with inert gas ion beams with optimized energy [72–75]. In particular, Ar ions with an energy of a few tens of eV proved able to almost double the sp^3/sp^2 ratio, while other inert gases (i.e., Xe), reactive gases (i.e., N_2, O_2) and Ar itself at different energy values were not as effective and, in some cases, even detrimental to the growing film [75].

Other variants of the standard technique have been tested, aiming to modify the LIP expansion dynamics and increase the ionization degree and ion bombardment by introducing additional excitation sources. For example, supporting the LIP expansion with magnetic fields can efficiently confine and drive the plasma ions to the substrate, and improvements both in terms of the sp^3 fraction and mechanical and morphological properties have been observed with respect to depositions carried out in the absence of magnetic fields [76,77].

Another approach, which aims to control the kinetic energy and ionization degree of the C plasma species, as well as reduce the density of molecular clusters, involves the use of laser pulse shaping and synchronous or temporally delayed double laser pulses to ablate the target [78,79]. Here, the expression "double laser pulses" is meant to indicate that both pulses are focused on the carbon source target, either at the same time or with a suitable inter-pulse delay. On the contrary, in "double laser beam" or "dual PLD", two different laser beams are focused on two different targets, so to produce a composite or doped DLC (see for example [80–84].

As an alternative to dual PLD, PLD assisted by magnetron sputtering has also been tested, where the second laser source is replaced by a DC magnetron providing a flow of dopant atoms [80,85,86].

Finally, providing additional energy to C adatoms by heating the substrate has also been tested, and proved ineffective at increasing the sp^3 fraction, as it appears to not only increase the film graphitization but also degrade its mechanical properties and surface quality [87–92]. As will be described in Section 4, in fact, this is an effective method to maximize the sp^2 fraction of the deposited films, which is undesirable in DLC but highly beneficial when the goal is depositing graphenic materials.

3.3. Type and Pressure of Background Gas

Emission spectroscopy of laser-induced plasmas, i.e., LIBS, clearly shows that the chemical nature and pressure of the background gas have a profound influence on the physical–chemical characteristics of the plasma in terms of ionization degree, expansion dynamics, persistence time and rate of elementary processes such as recombination and dissociation, both between the plasma species themselves and with the background en-

vironment [51,52]. It is no surprise, therefore, that another well-established approach to maximizing the sp^3 fraction is carrying out the depositions in an atmosphere containing reactive gases which can both affect the sp^3/sp^2 balance and be integrated as dopants in the growing film.

For PLD of DLC and related materials (such as nanocrystalline diamond), the most effective and widely used reactive gas is hydrogen, analogously to CVD of diamond films, which is usually carried out in a reactive atmosphere containing variable percentages of hydrogen. This gas plays a crucial role in diamond growth by selectively etching carbon atoms with sp^2 hybridization and stabilizing sp^3 bonds (see, for example, [93–98]).

An oxygen atmosphere has proved to be quite as efficient to increase the diamond fraction in the deposited film, though following a different mechanism [99–105].

Both gases can selectively etch sp^2-C, thus leaving a higher sp^3-C fraction in the film; but, while oxygen molecules react as such, and are therefore effective even at low pressure, only hydrogen atoms are reactive with sp^2-C. A higher hydrogen pressure is therefore needed for molecules to collide, dissociate and produce reactive atoms, which in turn can affect the deposition process by slowing down the C-plasma species and potentially limiting the sp^3-C percentage in the film.

Other reactive gases have also been used, such as hydrogen-containing gases (e.g., C_2H_2 [106], CH_4 [95,107]) and nitrogen [96–112]. Like molecular hydrogen itself, these gases can only interact with the growing films after dissociation; therefore, a careful optimization of their pressure is required to avoid too drastic a reduction of the kinetic energy of C ions.

Inert gases such as Ar and He are less appropriate, since their effect, especially at comparatively high pressure, mostly amounts to slowing down the C plasma species, thus increasing the density of molecular clusters and limiting the sp^3-C fraction in the deposited film. For example, in [113], Ar and He atmosphere at pressure higher than 200 mTorr yielded mostly sp^2-C films while, in [114], the deposits obtained in He in the pressure range from 0.6 Pa to 2 kPa consisted of various kinds of nanosized cluster-assembled carbon films.

3.4. Effect of Target and Substrate Quality, Distance and Relative Orientation

A high-quality surface of the target and substrate, as well as their respective distance and orientation, are other experimental parameters that can have a profound effect on the quality of films deposited by PLD, and this is especially true in the case of DLC.

Rough surfaces of the substrate and/or target are linked to a decrease in the diamond character, caused in both cases by a loss of kinetic energy of the ablated C species. Irregularities in the substrate surface can hinder the diffusion of C atoms reaching the substrate itself, thereby promoting their clustering and re-graphitization rather than the formation of smooth films with sp^3 bonds.

On the other hand, target surface inhomogeneity, either due to poor quality of the starting material or caused by the formation of craters upon prolonged laser ablation, can decrease the fluence of subsequent laser shots. This, too, can affect the plasma formation and expansion dynamics, thus in turn indirectly altering the properties of the deposited film [35]. Moreover, a coarse or heavily pitted surface is more prone to the ejection of clusters and particulates, which can reduce both the sp^3 fraction (since no $sp^2 \rightarrow sp^3$ transition occurs) and the smoothness of the deposited film.

Finally, both on-axis and off-axis deposition geometries have been attempted, yielding DLC films with different chemical, mechanical and electrical properties. As often observed in PLD, the best results in terms of film homogeneity and mechanical properties are obtained with off-axis configurations, in which the target and substrate are parallel but not coaxial. In the DLC case, this effect is even more marked, due to the sp^3 fraction relying strictly on the kinetic energy of the plasma species and on the absence of clusters. The plasma regions at small angles from the expansion axis are characterized by higher kinetic energy and lower density of clusters and particulates than those at larger angular distances; therefore, they are the most appropriate for growing high-sp^3-C films. As previously mentioned in Section 1, using an off-axis deposition configuration or mechanical shutters

to screen the substrate from the plasma regions at larger expansion angles can ensure better homogeneity, both morphological and chemical, of the deposited films [35,68]. Figure 5 summarizes the ways in which the experimental parameters discussed so far can affect the sp^3 fraction of DLC deposited by PLD, along with two examples of Raman spectra representing the two opposite outcomes of the process, i.e., one DLC film with a high sp^3 fraction and one disordered graphite film with zero sp^3 fraction.

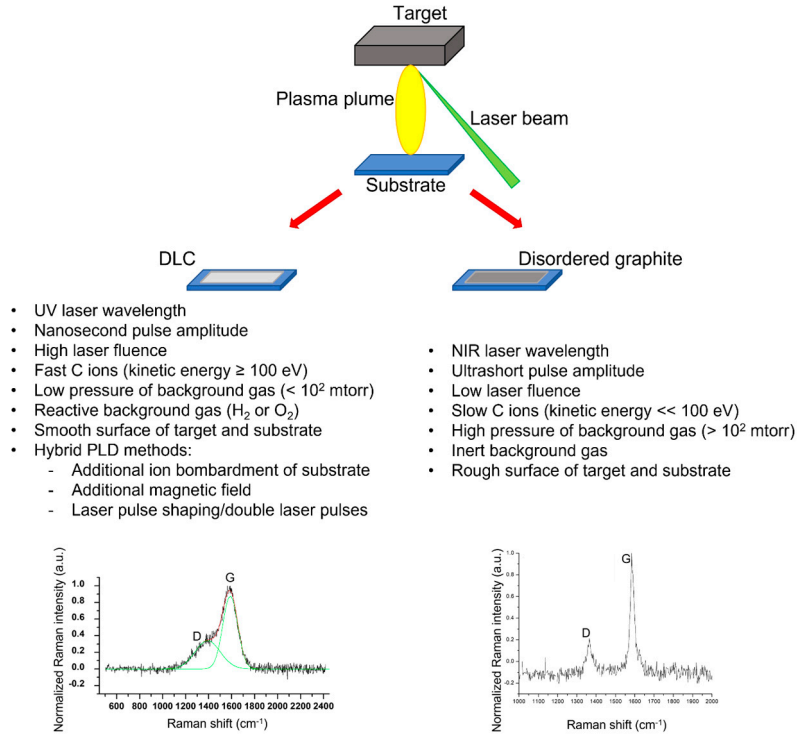

Figure 5. Summary of the effect of experimental parameters on the sp^3 fraction of DLC films deposited by PLD. The experimental parameters listed on the left are those able to promote the $sp^2 \rightarrow sp^3$ transition and, therefore, form DLC films with the characteristic Raman spectral features reported on the bottom left. The parameters listed on the right are those that proved ineffective at this task and are, therefore, associated with the deposition of mostly sp^2-C films with a degree of disorder induced by the laser ablation and deposition process. The Raman spectral features of disordered sp^2-C are reported on the bottom right. Despite the same D and G bands (whose origin is discussed in the text) are present in both cases, their aspect is profoundly different and clearly indicates the formation of two different kinds of materials. The Raman spectrum of DLC shows the deconvolution of the D and G peaks (in green), which are obtained with a two-Gaussian-peak fit (in red) and whose intensity ratio is one of the main diagnostic criteria for the sp^3-fraction evaluation (see text). Raman spectra images were adapted from [115].

The spectral features shown in this image are the so-called D and G bands (around, respectively, 1360 cm^{-1} and 1580 cm^{-1}).

These signals provide an indirect estimation of the sp^3 fraction because they both originate from sp^2-hybridized C atoms. The D band is due to a breathing mode of graphitic rings, which is absent in perfect graphite and only arises in the presence of disordered rings, while the G band results from an in-plane bond-stretching motion of pairs of sp^2-C atoms.

While crystalline diamond has a highly diagnostic Raman peak at 1332 cm^{-1}, which unequivocally indicates the presence of crystalline diamond domains, this is not usually observed in DLC spectra (and is, therefore, not reported here). This is because its cross section to excitation with visible and NIR radiation (the excitation sources customarily used in Raman spectroscopy) is 50–230 times lower than that of signals of graphitic materials.

Moreover, even in DLC films with high sp^3 content, the diamond domains are included in an amorphous matrix, rather than assembled in an orderly crystalline lattice.

Therefore, rather than observing a spectral feature directly related to the sp^3 hybridization, the $sp^2 \rightarrow sp^3$ transition is indirectly monitored through the evolution of the ratio between the D and G peaks intensity (I_D/I_G) and the variations in the G peak position along the amorphization trajectory, i.e., a three-stage model of bonding and ordering from graphite to tetrahedral amorphous C (ta-C) [116]. In [116], it is reported that, along the amorphization trajectory, these parameters do not change monotonically, but rather follow the trend reported in Figure 6a.

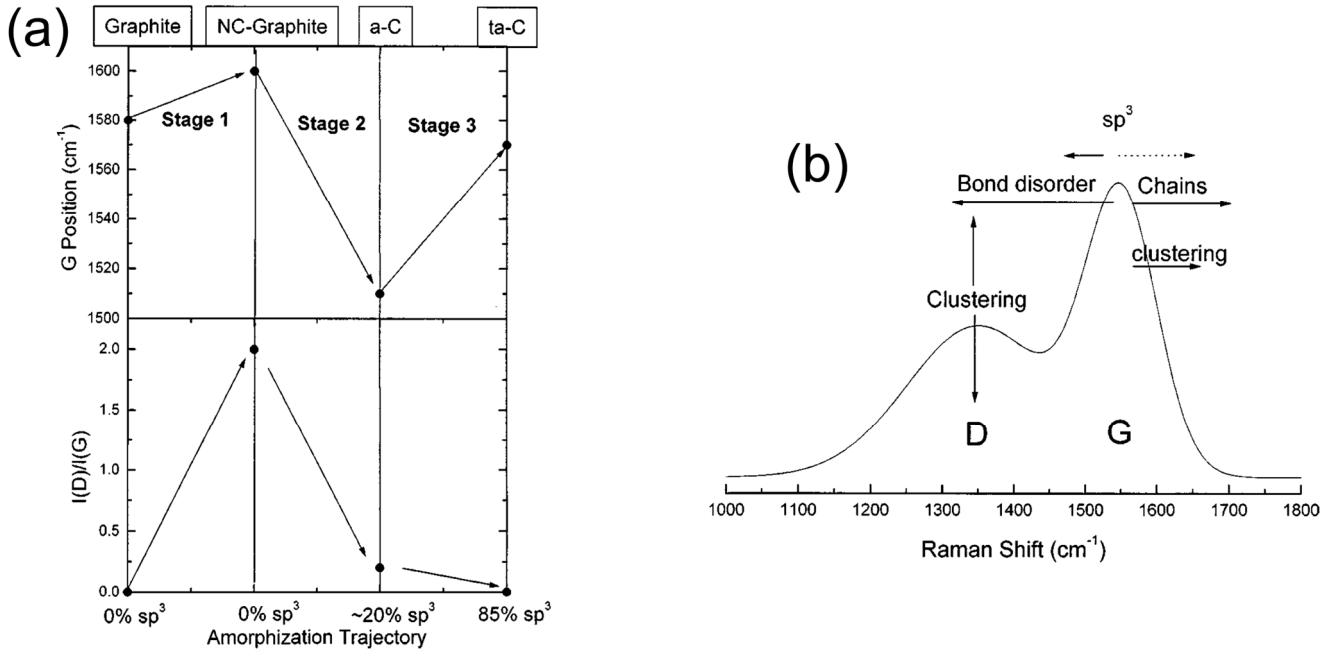

Figure 6. (**a**,**b**). (**a**) Schematic diagram of the three stages of the amorphization trajectory from crystalline graphite (100% sp^2) to tetrahedral amorphous C (100% sp^3). NC-Graphite, a-C and ta-C indicate, respectively, nanocrystalline graphite, amorphous carbon and tetrahedral amorphous carbon; (**b**) schematic diagram of factors affecting the height and position of the diagnostic D and G bands in the Raman spectra of DLC. Reproduced with permission [116]. Copyright year 2000, American Physical Society, APS. from APS.

The transformation from crystalline graphite (100% sp^2-C) to ta-C (100% sp^3-C, defected diamond) proceeds along the steps depicted in Figure 6a, while Figure 6b schematically shows how other factors such as the degree of clustering and bond disorder can affect the I_D/I_G ratio and the G peak shift.

4. PLD of Graphene

While in DLC the main goal of PLD techniques is promoting a transition from thermodynamically stable graphite, where C is sp^2-hybridized, to kinetically favored diamond, where C is sp^3-hybridized, the deposition of graphene aims to generate sheets of C atoms with purely sp^2 hybridization with a honeycomb arrangement.

Since its discovery in the 2000s [117,118], and thanks to its unique electronic, thermal, mechanical and chemical properties, graphene has been attracting extremely intense research interest aiming to synthetize this C allotrope with exceptional heat and electricity conductivity, optical transparency and strength with a vast array of potential applications in the most disparate fields (some of which are briefly summarized in Table 2).

Table 2. Mechanical, thermal and optical properties of single-layer graphene and a list of possible applications [119,120].

Properties of Single-Layer Graphene	Applications
High mechanical strength (42 N/m)	• Wear-resistant coatings • Enhanced construction materials
High elastic modulus (1 TPa)	• Flexible, wearable electronics
High specific surface area (2630 m^2/g)	• Electrode material • Gas sensors
High carrier mobility (2×10^5 $cm^2/V*s$)	• Fast electronics • Supercapacitors
High transparency (97.7%)	• Transparent protective coatings • Transparent photovoltaics
High thermal conductivity (5000 W/m*K)	• High-heat-dissipation coatings • Improved heat management and distribution
Chemical stability Biocompatibility Resistance to oxidation and corrosion	• Biosensors • Anti-biofilm coatings • Anti-corrosion coatings
Hydrophobicity	• Water-repellent coatings

The properties of multilayer graphene approach those of bulk graphite when the number of layers exceeds 5; therefore, significant research efforts are aimed at developing chemical and physical methods for the deposition of few-layer or, ideally, monolayer graphene films.

The main techniques that are currently employed to produce graphene include exfoliation of graphite (either by mechanical or chemical means), CVD and reduction of graphene derivatives such as graphene oxide and fluorographene via chemical, electrochemical, thermal or photocatalytic routes [119] (and references therein).

In addition to the general features mentioned in Section 1, PLD has some specific advantages when compared to CVD and other PVD methods which are particularly useful for the deposition of graphene. These include the good adhesion to the substrate, milder deposition conditions (specifically, lower substrate temperature and lower vacuum) and better film stoichiometry control, including when dopants need to be incorporated into the growing film. Moreover, with respect to more traditional methods such as mechanical exfoliation and CVD, PLD enables the growth of graphene films on relatively large areas, on virtually any kind of substrate and with a higher growth rate, thus providing a comparatively facile and inexpensive route to the desired material [34] (and references therein).

The following sections describe the main PLD methods that have been reported in the literature for the deposition of graphene and its derivatives (graphene oxide, hydrogenated graphene, doped graphene), with a focus on the experimental parameters that have proved able to provide fewer-layer, higher-quality films.

4.1. PLD of Graphene with and without Metal Catalysts

Two main approaches have been tested for PLD of graphene: one that involves the use of metallic catalysts deposited on the substrate in different phases of the film growth, and one that proceeds without catalysts. The latter approach is particularly attractive as it eliminates the need to transfer the deposited graphene film and to grow it, in principle, directly on any desired substrate (e.g., pure and doped Si, SiO_2 and fused silica [121–129], sapphire [130], copper [131–133], glass [134]). In fact, considerations such as substrate–film

lattice mismatch and film–substrate adhesion should, as usual with thin-film deposition techniques, always be considered when producing usable films for specific applications is the goal.

In this view, it has often been observed that higher-quality graphene films, featuring fewer defects and a reduced number of layers, can be grown with metallic catalysts, and this experimental approach is, therefore, more common. For this reason, and due to the specificities of the mechanisms of graphene growth in the presence of catalysts, in the remainder of this section the discussion will describe PLD of graphene with catalysts in more detail than the catalyst-free approach. The results of the catalyst-free articles referenced above will be addressed also in the following sections, along with the effect of the additional experimental parameters investigated in these works.

The most widespread catalyst for PLD of graphene is Ni, which is deposited as a thin film on the substrate, typically via PLD, thermal evaporation or sputtering. Two main relative arrangements of graphene and Ni are possible, i.e., the catalyst can be deposited either (1) directly on the substrate prior to the deposition of graphene [134–138] or (2) subsequently, on top of the graphene layer [139–141]. Some authors also used a double-layer geometry, i.e., they carried out the Ni/graphene deposition process twice and obtained two superposed catalyst/film layers [142]. This enabled depositing smoother catalytic layers with fewer grain boundaries and, in turn, graphene films with large area and low density of defects.

In all these cases, as well as in the absence of catalysts, the substrate temperature and its controlled variations play a crucial role in defining the properties of the deposited graphene films. The substrate is usually kept at high temperature (from several hundreds of °C up to 1300 °C, though room-temperature depositions have also been reported) so to provide the C plasma species impinging on the substrate with enough kinetic energy to reach thermodynamically stable sites, bond on the graphene sheet edge and grow ordered few-layer graphene rather than forming randomly oriented covalent bonds.

The latter behavior is often observed at low substrate temperatures and is associated with higher density of defects and an increasingly amorphous character, as evidenced by various microscopy techniques and Raman spectroscopy (see, for example, [123,125,127,130].

After the deposition, a sequence of thermal annealing and subsequent cooling is carried out, which serves a different purpose depending on the chosen catalyst/graphene film configuration. When the carbon film is grown directly on the substrate and then covered with the catalyst film (Figure 7a), the thermal treatment allows first the diffusion of carbon atoms through the metallic layer (annealing) and then, in the cooling phase, it promotes the precipitation and formation of the graphene film by exploiting the temperature-related decrease in solubility of C into Ni [143,144]. In the opposite configuration, where the catalyst film is deposited first, the thermal treatment is used to convert the amorphous carbon film, initially formed on top of the Ni layer and containing an amorphous mixture of sp^2- and sp^3-C, into few-layer graphene. Moreover, by heating the Ni layer during the C layer deposition, the grain size of the Ni film can be increased, thus in turn promoting the formation of graphene films with larger grain size and fewer layers.

While some authors reported the growth of graphene films at relatively low (250 °C, on Sn [145]) or room temperature (on composite Ni-Cu catalytic substrates [146]), higher substrate temperature is generally reported as resulting in higher-quality graphene films [34].

Another important parameter to control during the post-deposition thermal treatment is the cooling rate. In [147], it was shown that—not only with Ni, by far the most widespread catalyst for PLD of graphene, but also with other metals (e.g., Co)—increasing the cooling rates ensured better quality films with fewer layers and lower defect density. On the other hand, both substrate temperature and cooling rate appear to require careful optimization to identify the optimal range of values, since it was also observed that no graphene formation could be obtained with very high cooling rate (i.e., 100 °C/min) [147] and that the benefits of increasing the substrate temperature and annealing conditions were not universal but, rather, substrate-dependent [135,139].

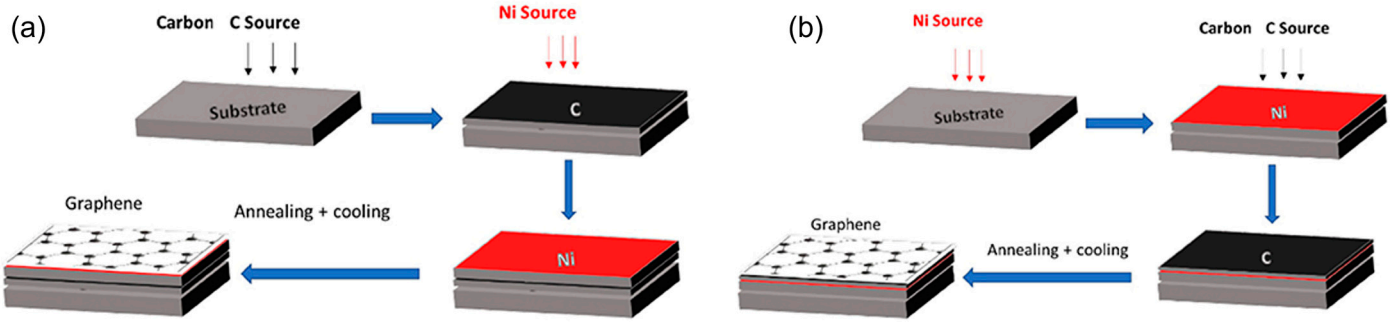

Figure 7. (**a**–**b**) Different configurations for PLD of graphene with a Ni catalyst: (**a**) an amorphous C layer is deposited on the substrate prior to the deposition of the catalytic Ni layer; (**b**) an amorphous C layer is deposited on top of the previously deposited catalytic Ni layer. Adapted from [34], Copyright 2018 Bleu, Bourquard, Tite, Loir, Maddi, Donnet and Garrelie.

Since the precipitation of a continuous graphene film on top of the catalyst layer is due to the diffusion of C atoms in the metallic layer [147], the relative thickness of the two layers is also an important parameter that can be optimized by acting on laser parameters (repetition rate, fluence) and deposition conditions (ablation time, thickness of the catalyst layer, annealing temperature). In [136], for example, it was observed that a low C-to-Ni thickness ratio produced the desired few-layer graphene (down to two layers), while multilayer graphene was obtained with a higher C-to-Ni thickness ratio. Bilayer graphene (and a small percentage of monolayer graphene) was also deposited in [126], where the authors found that the best conditions to deposit bilayer graphene combined an optimal amorphous C-to-Ni thickness ratio with high-temperature and rapid annealing.

Among the studies that report the formation of graphene films at low or room temperature, some introduced additional experimental variables in the standard deposition technique. For example, Larki et al. [138] found that, thanks to the effect exerted by magnetic fields on the plasma plume species, by using stronger stationary magnets they could produce fewer-layer, fewer-defect graphene films than with weaker magnets or without magnetic fields at all.

The effect of adding a supporting DC bias to the substrate holder was investigated in [148], where the authors aimed to deposit n-doped graphene-like carbon nitride films by carrying out the deposition in a N_2-containing atmosphere. While improving the N incorporation in the growing film, the DC bias was found to negatively affect the overall quality of the film in terms of increased disorder and deterioration of the film's electrical properties.

In general, introducing a background gas and tailoring its composition proved a very efficient strategy for the room-temperature deposition of graphene and graphene oxide [125,133], as will be discussed in more detail in Section 4.3.

4.2. Effect of Laser Parameters and Deposition Conditions

The use of PLD for graphene synthesis is a rather recent implementation of this technique. Therefore, while the effect of laser parameters such as wavelength, pulse amplitude and repetition rate for DLC has been studied by several groups throughout the decades, and clear indications have emerged about the most suitable conditions for the deposition of this material, in the case of graphene the implications of different laser sources on the quality of the growing film have not yet unequivocally been elucidated.

The first attempts at the growth of graphene films were made with the fundamental and second harmonic of nanosecond Nd:YAG lasers (respectively, 1064 nm and 532 nm) [121,122,149,150], and several recent works have also employed them [134,135,151,152].

Recent research on PLD of graphene has also largely explored UV laser sources; in particular, KrF excimer lasers at 248 nm [123,124,126,127,131,132,137–139,141,153] and, occasionally, the higher harmonics of Nd:YAG lasers (355 nm [129], 266 nm [133]). The

reports of graphene films grown with femtosecond lasers, mostly Ti:Sapphire at 800 nm, are also sporadic [140,148], as they do not appear to provide significant advantages with respect to longer-pulse sources, while remaining generally more expensive and less user-friendly.

Parameters such as laser fluence and repetition rate are optimized in each experiment and with the specific employed setup, but some general trends can be inferred as to how some experimental parameters can affect the graphene film. As mentioned in the previous section, evidence has emerged that controlling the number of laser pulses reaching the target (by acting on the laser repetition rate and the ablation time) can affect the C-to-metal thickness ratio and is therefore key to obtaining few-layer graphene films [131,136].

The recent study by Wang et al. [132] reported the deposition of monolayer and bilayer graphene on a crystalline Cu substrate with a KrF laser by acting on two main parameters: substrate temperature and laser fluence. Based on their results, the authors suggested the existence of a threshold value for the laser fluence, which determines the number of graphene layers in the deposited film. This is due to changes in the amount of kinetic energy of the C plasma species and, consequently, in the balance between their diffusion and condensation at the substrate surface. Below the threshold, the deposited films mostly consisted of high-quality monolayer graphene because the deposited C atoms forming the first graphene "islands" have enough energy to diffuse and join other islands rather than grow on top of underlying forming layers. On the other hand, above the threshold, the formation of bilayer graphene prevails because, due to the higher laser density, the number of incoming C atoms also increases and condensation dominates over diffusion.

The possible existence of a laser energy threshold is also suggested by the work of Ershov et al. [151,152], which showed that increasing the energy density of a 20 ns Nd:YAG laser caused an increase in defects and the formation of smaller sp^2 crystallites in graphenic films deposited on metallic and metal-oxide substrates. These works, unlike most other examples of PLD of graphene and graphene-like materials, were not carried out in vacuum or a reduced pressure atmosphere, but in He at atmospheric pressure, and by using a sacrificial nanocarbon tape as the target rather than graphite.

Sarath Kumar and Alshareef [127] showed that, in the absence of a catalyst, the higher fluence of a 20 ns KrF laser produced graphene films with fewer layers and more defects, irrespective of the employed substrate. On the other hand, the number of layers and density of defects showed a strong dependence on the substrate temperature, with no graphene films grown at temperatures lower than 700 °C.

Figure 8 summarizes the effects of various experimental parameters on the number of layers of graphene deposited by PLD. Two examples of Raman spectra of multilayer and monolayer graphene are also reported, which display the three most diagnostic spectral features, i.e., the D, G and 2D bands (around, respectively, 1360 cm^{-1}, 1580 cm^{-1} and 2730 cm^{-1}).

The origin of D and G bands has already been discussed in Section 3.4. The 2D band (also known as G' band) is closely related to the formation of graphene, and its shape (particularly, symmetry—or lack thereof—and number of convoluted sub-peaks forming the overall band) and intensity ratio to the G band (I_{2D}/I_G) provide an indication of the number of graphene layers. Generally speaking, the higher the I_{2D}/I_G value, the lower the number of graphene layers. Values of I_{2D}/I_G lower than ~0.3 indicate the formation of multilayer graphene, while values higher than ~0.4 signal the formation of few-layer graphene (<5 layers). Monolayer graphene has I_{2D}/I_G >0.5 and a 2D band that is made up by a single peak, while bilayer graphene is made up by four sub-peaks [154].

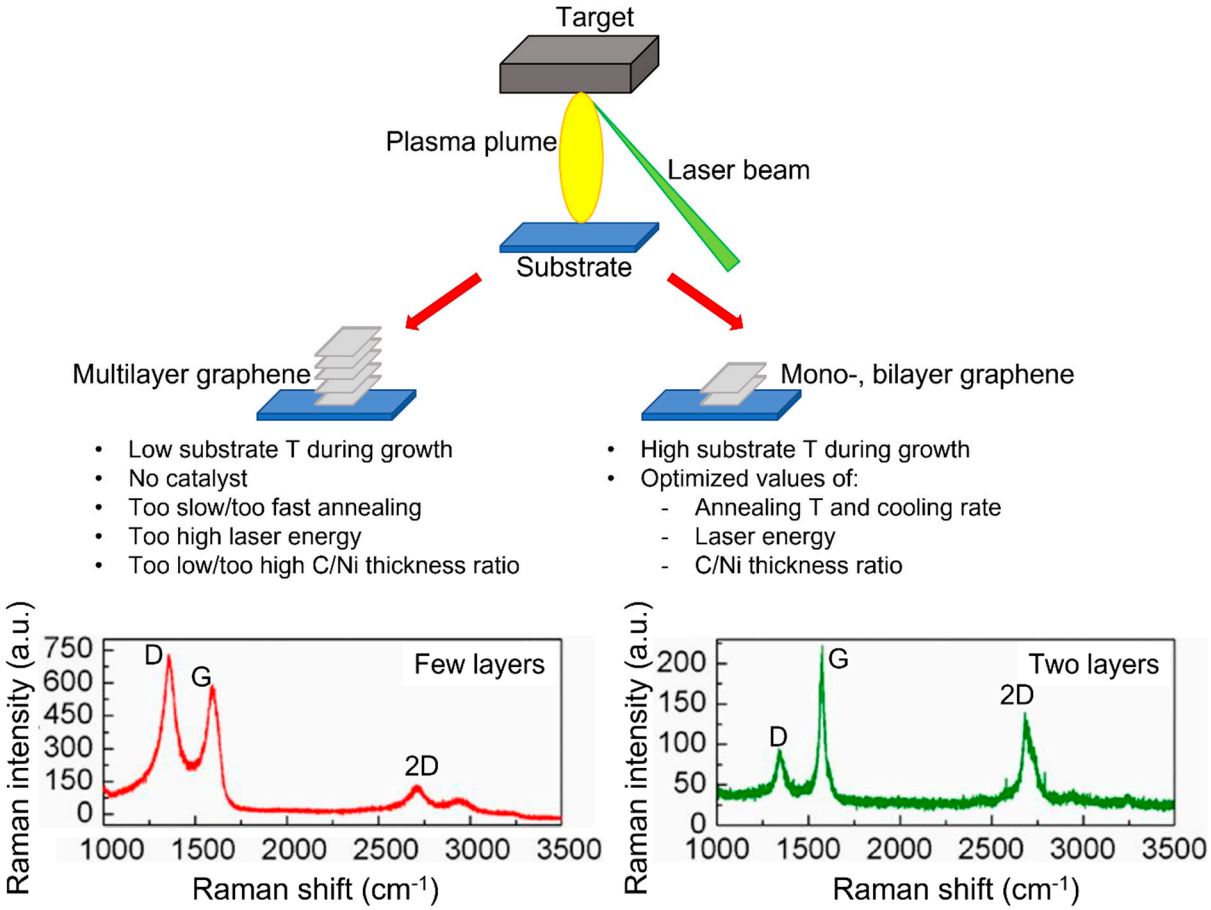

Figure 8. Summary of the effect of experimental parameters on the kind of graphene deposited by PLD. The parameters listed on the left can promote the growth of multilayer graphene, while those on the right enable the formation of mono- and bilayer graphene (usually the desired outcome). The Raman spectra of both kinds of graphene, reported at the bottom, display the typical D, G and 2D graphene bands. The I_{2D}/I_G ratio provides a direct indication of the number of layers, as higher I_{2D}/I_G values correspond to fewer layers (see text for details). Raman spectra images adapted from [136].

4.3. PLD of Graphene Derivatives

As described in the previous section, deposition of pristine graphene is usually carried out in vacuum, but several works report using a background gas, especially when the goal is incorporating dopants in the growing film or producing graphene derivatives.

N-doped graphene was obtained by carrying out the deposition in a nitrogen atmosphere, both with a Ni catalyst layer [137,140,148] and without metallic catalysts [124,153]. It is worth mentioning that both n-doped and p-doped graphene have also been obtained by co-ablation of nitrogen/boron and carbon targets [155], or ablation of carbon targets containing the desired dopant [140], rather than using nitrogen/boron-containing reactants as gaseous precursors as is usual in CVD.

The amount of incorporated dopant can be tailored either by controlling the pressure of the gas, in cases when the deposition is carried out in a gaseous atmosphere containing the desired dopant, or by controlling the ablation time and stoichiometry of the dopant-containing target. Multilayer graphene oxide [125] and hydrogenated graphene [123] have been grown catalyst-free by using, respectively, oxygen and hydrocarbons (e.g., CH_4) as background gases. Both works studied the effect of substrate temperature on the deposited films while keeping all other experimental parameters constant and confirmed that, at low temperatures, the deposited material tends to be an amorphous mixture of sp^2/sp^3-C

rather than graphenic in nature. In [125], graphene oxide was produced only at substrate temperatures of 400 °C and higher, while lower temperatures promoted the formation of amorphous C films with lower crystallinity and different wettability behavior (hydrophilic as opposed to the usual hydrophobic character of graphene oxide). Similarly, in [123], when the substrate temperature was increased from room temperature to 400 °C, a transition took place from amorphous hydrogenated C films to a hydrogenated graphene structure, while a further temperature increase caused film dehydrogenation and a higher number of defects.

Sarath Kumar and Alshareef [127] found that graphene could be grown catalyst-free and at high substrate temperature, but only in 20 mTorr Ar, while the same pressure of oxygen led to the formation of graphitic oxides entirely devoid of the Raman spectral signatures of graphene and graphene-like films. In a subsequent work, they tested both Ar and N_2 as background gases, at the same pressure, and were able to deposit p-doped and n-doped graphene and to produce an entirely PLD-deposited, graphene-based diode [153].

Unlike that reported in [127], the use of variable mixtures of Ar and O_2 at fixed total pressure of 20 mTorr was found to be highly beneficial in the recent investigation by Juvaid et al. [133], who developed a single-step, catalyst-free, no-annealing process for the deposition of reduced graphene oxide on various metals and semiconductors with the fourth harmonic of a nanosecond Nd:YAG laser (266 nm). By finely tuning the partial pressures of the two gases, the authors found that the optimal conditions for the growth of highly homogeneous reduced graphene oxide films were those with O_2 partial pressure lower than 2 mTorr, which allowed for maximizing the sp^2-C amount in the film and benefited from the reduced kinetic energy of C plasma species due to the relatively high partial pressure of the inert gas (18 mTorr).

Some groups have also proposed an interesting kind of graphene-derived material, i.e., graphene films functionalized with nanoparticles (NPs) to obtain hybrid materials with enhanced catalytic, electric and sensing properties with respect to the pristine material [156]. Tite et al. [141] used a typical PLD experimental configuration (high vacuum, Si substrate, Ni catalyst deposited on top of the carbon film, excimer nanosecond laser) to prepare few-layer graphene films by depositing amorphous carbon films and then annealing them. They then decorated the obtained films by drop-casting Au NP colloidal solutions and, thus, produced substrates for Surface-Enhanced Raman Scattering (SERS) with good spectroscopic enhancement capabilities.

Porous graphene layers with increased catalytic activity for methanol dissociation were instead prepared in [157], where the authors deposited ceria NPs via PLD onto CVD-produced graphene films.

5. PLD of Carbyne/Carbon-Atom Wires (CAW)

The third hybridization that carbon atoms can acquire is sp. While the allotropes in which C atoms have sp^2 and sp^3 hybridizations are nowadays well known and the existence of several of their derivatives has been experimentally and theoretically proved, the same may not be said for the still hypothetical C allotrope having an sp hybridization.

The literature has referred to this elusive material with various names, of which the most recurrent are carbyne and carbon-atom wires, while chaoite or white carbon indicate natural or synthetic minerals made of mostly sp-carbon. Carbyne is a (hypothetical) 1D material formed by single carbon atom chains with sub-nanometric diameter and infinite length, while real-life 1D wires of finite lengths are referred to as carbon-atom wires (CAW).

Two possible bonding schemes are possible, i.e., alternating single and triple bonds, such as in polyynes, and consecutive double bonds between each carbon atom, such as in cumulenes (Figure 9).

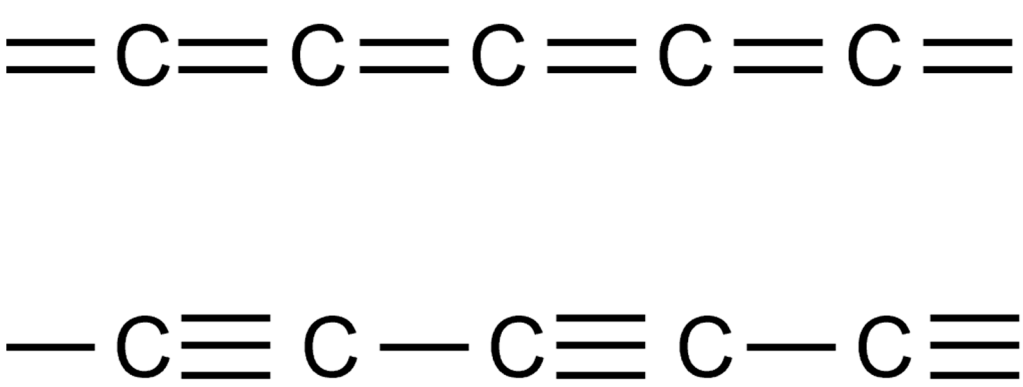

Figure 9. Cumulene-like (**top**) and polyyne-like (**bottom**) possible structures of carbyne.

Despite the existence of this material in the condensed phase is still disputed, and it is therefore very far from being potentially exploited for practical applications as is already happening for its sp^2- and sp^3-hybridized counterparts, carbyne is still worth a brief mention in this review, since laser-based methods are among those employed in the quest for this yet unknown carbon allotrope. For details about the structure, properties and detection of CAW, interested readers may refer to two recent papers by Casari et al., one review [36] and one perspective article [158].

In addition to bottom-up synthetic routes [36] (and references therein), several laser-based methods have also been proposed to produce carbynous materials. These methods include laser irradiation of graphite targets in a vacuum or inert gas background [159–161] and actual PLD on a substrate [162,163]. Finally, stable colloidal solutions of polyyne wires, which can be considered carbyne precursors, have been obtained by Pulsed Laser Ablation in Liquids (PLAL) where, as briefly mentioned in Section 1, the laser beam generates a plasma at the surface of a submerged target. The plasma generated in PLAL, therefore, expands against a liquid bulk, forming cavitation bubbles and generating a peculiar reaction environment with extreme conditions of pressure and temperature [58–60].

For the synthesis of polyynes, this technique has been applied by ablating either submerged graphite targets [164,165] or liquid dispersions of carbon-containing nanomaterials [166–169]. The main advantage of laser-based techniques with respect to chemical synthesis of polyynes is the fact that they are scalable and experimentally more flexible and safer (CAWs are extremely unstable materials [170]), though the tradeoff is that the obtained materials are usually not pure sp-C, but rather mixtures of varying percentages of sp-C embedded in sp^2-C or sp^3-C matrices.

6. Conclusions and Perspectives

The extraordinary flexibility of PLD has been its boon and bane in the field of material science. On one hand, the possibility of independently changing virtually all experimental parameters, such as laser features (wavelength, irradiance/fluence, pulse amplitude), background gas (kind, composition and pressure), target and substrate (chemical nature, temperature, distance and relative deposition geometry), additional apparatus modules (magnetic fields, multiple laser pulses, DC or RF discharges) can make the fine control of the conditions and meaningful comparisons between research results of different groups a rather complicated task. At the same time, it offers vast opportunities for tailoring the deposition process and giving many important contributions both to applied material science and to fundamental research.

In this article, these inherent characteristics of PLD have been reviewed within the specific frame of the production of thin films of carbon-based materials, with a focus on three representative examples of sp^3, sp^2 and sp hybridizations of this element, i.e., diamond-like carbon (DLC), graphene and carbyne.

DLC is one the most studied research applications of PLD, and this paper reviewed the experimental trends that emerged in the literature of the last two decades to promote

the $sp^2 \rightarrow sp^3$ transition by laser ablation of graphite targets, with the goal being to obtain films with mechanical and physical-chemical properties similar to natural diamond. The discovery of graphene and its recognition as a carbon allotrope is a more recent scientific endeavor, and PLD has demonstrated that it can successfully compete with well-established chemical and physical deposition techniques to obtain high-quality films of this extraordinary material. In fact, PLD of graphene and its derivatives (graphene oxide, doped graphene) is an extremely active area of research in which the milder experimental conditions and great tailorability of this technique can be expected to play an important role in the future massive transition of graphene from research to everyday applications in various industries (first and foremost, electronics and biomedical).

On the other hand, the so-called "lacking allotrope"—i.e., sp-hybridized carbyne and its real-world counterpart, carbon atom wires (CAW)—is cutting-edge fundamental research, since its existence as an actual carbon allotrope is still disputed. Research efforts focusing on the production of sp-only carbon materials range from wet chemistry to physical vapor deposition methods, and PLD and other laser-based techniques (PLAL and laser evaporation) are providing important contributions in the search for this elusive material.

From the industrial applications point of view, the deposition of thin films is an important technological niche, where PLD has nonetheless not yet acquired a primary role, despite important progress having been demonstrated, especially for piezoelectric oxides and ceramics for microelectronic [171] and photovoltaic [172] applications; tribological coatings [173]; and 2D materials, including graphene, for high-performance photodetectors [174]. This is likely due to two main inherent limitations, which have so far limited its penetration in the industrial world and which future research should address in order to promote the transition from small-scale research method to industry-ready mature technology. These are its low throughput and the relative lack of standardization of experimental apparatuses and conditions [31]. It can be envisioned that the commercial availability of deposition chambers, which several companies are currently marketing both for research labs and for large-area PLD, while possibly limiting the flexibility of the setup, will nonetheless significantly improve the reproducibility of results between different groups, thus favoring the commercial diffusion of PLD. Improving the throughput—and, therefore, the scalability—will likely require a concerted effort of PLD researchers to develop novel experimental approaches and the laser industry to provide high-frequency laser sources more suitable for the coverage of large areas with the desired thin films.

Finally, the possibility of carrying out online process diagnostics by optical emission spectroscopy of the plasma plume (i.e., LIBS, also called LIPS in the atomic spectroscopy literature) is an important advantage that should not be neglected. The experimental conditions used for PLD (vacuum or sub-atmospheric pressure of reactive or inert gases) are ideal for the observation of intense LIBS spectra which can provide extremely valuable information about the plasma composition and evolution, which can in turn be used both in the process optimization phase and in the online monitoring of the process itself, even in industrial settings.

Funding: This research received no external funding.

Data Availability Statement: No new data were created or analyzed in this study. Data sharing is not applicable to this article.

Conflicts of Interest: The author declares no conflict of interest.

References

1. Levi, P. *The Periodic Table*; Penguin Publishing: London, UK, 1975.
2. Thapliyal, V.; Alabdulkarim, M.E.; Whelan, D.R.; Mainali, B.; Maxwell, J.L. A concise review of the Raman spectra of carbon allotropes. *Diam. Relat. Mater.* **2022**, *127*, 109180. [CrossRef]

3. dos Santos, M.C.; Maynart, M.C.; Aveiro, L.R.; da Paz, E.C.; dos Santos Pinheiro, V. Carbon-Based Materials: Recent Advances, Challenges, and Perspectives. In *Reference Module in Materials Science and Materials Engineering*; Elsevier: Amsterdam, The Netherlands, 2017.
4. Saba, N.; Jawaid, M.; Fouad, H.; Alothman, O.Y. Nanocarbon: Preparation, properties, and applications. In *Nanocarbon and Its Composites*; Khan, A., Jawaid, M.I., Asiri, A.M., Eds.; Woodhead Publishing Series in Composites Science and Engineering; Woodhead Publishing: Sawston, UK, 2019; pp. 327–354.
5. Stankovich, S.; Dikin, D.A.; Piner, R.D.; Kohlhaas, K.A.; Kleinhammes, A.; Jia, Y.; Wu, Y.; Nguyen, S.B.T.; Ruoff, R.S. Synthesis of graphene-based nanosheets via chemical reduction of exfoliated graphite oxide. *Carbon* **2007**, *45*, 1558–1565. [CrossRef]
6. Chalifoux, W.A.; Tykwinski, R.R. Synthesis of extended polyynes: Toward carbyne. *Comptes Rendus Chimie* **2009**, *12*, 341–358. [CrossRef]
7. Chalifoux, W.A.; Tykwinski, R.R. Synthesis of polyynes to model the sp-carbon allotrope carbyne. *Nat. Chem.* **2010**, *2*, 967–971. [CrossRef]
8. Vetter, J. 60 years of DLC coatings: Historical highlights and technical review of cathodic arc processes to synthesize various DLC types, and their evolution for industrial applications. *Surf. Coat. Technol.* **2014**, *257*, 213–240. [CrossRef]
9. Manawi, Y.M.; Ihsanullah; Samara, A.; Al-Ansari, T.; Atieh, M.A. A Review of Carbon Nanomaterials' Synthesis via the Chemical Vapor Deposition (CVD) Method. *Materials* **2018**, *11*, 822. [CrossRef]
10. Cai, Z.; Liu, B.; Zou, X.; Cheng, H.-M. Chemical Vapor Deposition Growth and Applications of Two-Dimensional Materials and Their Heterostructures. *Chem. Rev.* **2018**, *118*, 6091–6133. [CrossRef] [PubMed]
11. Sivamaran, V.; Balasubramanian, V.; Gopalakrishnan, M.; Viswabaskaran, V.; Gourav Rao, A.; Selvamani, S. Carbon nanotubes, nanorings, and nanospheres: Synthesis and fabrication via chemical vapor deposition—A review. *Nanomater. Nanotechnol.* **2022**, *12*, 18479804221079495. [CrossRef]
12. Wang, X.; Sui, X.; Zang, S.; Yan, M.; Yang, J.; Hao, J.; Liu, W. Effect of deposition pressures on uniformity, mechanical and tribological properties of thick DLC coatings inside of a long pipe prepared by PECVD method. *Surf. Coat. Technol.* **2019**, *375*, 150–157. [CrossRef]
13. Li, A.; Li, X.; Wang, Y.; Lu, Z.; Wang, Y.; Zhang, G.; Wu, Z. Investigation of mechanical and tribological properties of super-thick DLC films with different modulation ratios prepared by PECVD. *Mater. Res. Express* **2019**, *6*, 086433. [CrossRef]
14. Devi, M.; Rawat, S.; Sharma, S. A comprehensive review of the pyrolysis process: From carbon nanomaterial synthesis to waste treatment. *Oxf. Open Mater. Sci.* **2021**, *1*, itab014. [CrossRef]
15. Aguilar-Elguézabal, A.; Antúnez, W.; Alonso, G.; Paraguay Delgado, F.; Espinosa, F.; Miki-Yoshida, M. Study of carbon nanotubes synthesis by spray pyrolysis and model of growth. *Diam. Relat. Mater.* **2006**, *15*, 1329–1335. [CrossRef]
16. Illakkiya, J.T.; Rajalakshmi, P.U.; Oommen, R. Nebulized spray pyrolysis: A new method for synthesis of graphene film and their characteristics. *Surf. Coat. Technol.* **2016**, *307*, 65–72. [CrossRef]
17. Cai, J.; Han, X.; Wang, X.; Meng, X. Atomic Layer Deposition of Two-Dimensional Layered Materials: Processes, Growth Mechanisms, and Characteristics. *Matter* **2020**, *2*, 587–630. [CrossRef]
18. Vervuurt, R.H.J.; Kessels, W.M.M.; Bol, A.A. Atomic Layer Deposition for Graphene Device Integration. *Adv. Mater. Interfaces* **2017**, *4*, 1700232. [CrossRef]
19. Xiao, Z.; Kisslinger, K.; Monikandan, R. Atomic Layer Deposition of Nanolayered Carbon Films. *C* **2021**, *7*, 67. [CrossRef]
20. Marichy, C.; Pinna, N. Carbon-nanostructures coated/decorated by atomic layer deposition: Growth and applications. *Coordin. Chem. Rev.* **2013**, *257*, 3232–3253. [CrossRef]
21. Chowdhury, S.; Laugier, M.T.; Rahman, I.Z. Characterization of DLC coatings deposited by rf magnetron sputtering. *J. Mater. Process. Technol.* **2004**, *153–154*, 804–810. [CrossRef]
22. Fiaschi, G.; Rota, A.; Ballestrazzi, A.; Marchetto, D.; Vezzalini, E.; Valeri, S. A Chemical, Mechanical, and Tribological Analysis of DLC Coatings Deposited by Magnetron Sputtering. *Lubricants* **2019**, *7*, 38. [CrossRef]
23. Stankus, V.; Vasiliauskas, A.; Guobienė, A.; Andrulevičius, M.; Meškinis, Š. Direct synthesis of graphene on silicon by reactive magnetron sputtering deposition. *Surf. Coat. Technol.* **2022**, *437*, 128361. [CrossRef]
24. Nakajima, Y.; Murata, H.; Saitoh, N.; Yoshizawa, N.; Suemasu, T.; Toko, K. Low-Temperature (400 °C) Synthesis of Multilayer Graphene by Metal-Assisted Sputtering Deposition. *ACS Omega* **2019**, *4*, 6677–6680. [CrossRef] [PubMed]
25. Presel, F.; Tetlow, H.; Bignardi, L.; Lacovig, P.; Tache, C.A.; Lizzit, S.; Kantorovich, L.; Baraldi, A. Graphene growth by molecular beam epitaxy: An interplay between desorption, diffusion and intercalation of elemental C species on islands. *Nanoscale* **2018**, *10*, 7396–7406. [CrossRef] [PubMed]
26. Lopes, J.M.J. MBE Growth of Graphene. In *Molecular Beam Epitaxy: Materials and Applications for Electronics and Optoelectronics*; Asahi, H., Horikoshi, Y., Eds.; John Wiley & Sons Ltd.: Hoboken, NJ, USA, 2019; pp. 395–409.
27. Albar, J.D.; Summerfield, A.; Cheng, T.S.; Davies, A.; Smith, E.F.; Khlobystov, A.N.; Mellor, C.J.; Taniguchi, T.; Watanabe, K.; Foxon, C.T.; et al. An atomic carbon source for high temperature molecular beam epitaxy of graphene. *Sci. Rep.* **2017**, *7*, 6598. [CrossRef]
28. Chrisey, D.B.; Hubler, G.K. (Eds.) *Pulsed Laser Deposition of Thin Films*; John Wiley & Sons: Hoboken, NJ, USA, 1994.
29. Eason, R. (Ed.) *Pulsed Laser Deposition of Thin Films: Applications-Led Growth of Functional Materials*; John Wiley & Sons Inc.: Hoboken, NJ, USA, 2006.

30. Ashfold, M.N.R.; Claeyssens, F.; Fuge, G.M.; Henley, S.J. Pulsed laser ablation and deposition of thin films. *Chem. Soc. Rev.* **2004**, *33*, 23–31. [CrossRef] [PubMed]
31. Shepelin, N.A.; Tehrani, Z.P.; Ohannessian, N.; Schneider, C.W.; Pergolesi, D.; Lippert, T. A practical guide to pulsed laser deposition. *Chem. Soc. Rev.* **2023**, *52*, 2294–2321. [CrossRef]
32. Masood, K.B.; Kumar, P.; Malik, M.A.; Singh, J. A comprehensive tutorial on the pulsed laser deposition technique and developments in the fabrication of low dimensional systems and nanostructures. *Emergent Mater.* **2021**, *4*, 737–754. [CrossRef]
33. Haider, A.J.; Alawsi, T.; Haider, M.J.; Taha, B.A.; Marhoon, H.A. A comprehensive review on pulsed laser deposition technique to effective nanostructure production: Trends and challenges. *Opt. Quant. Electron.* **2022**, *54*, 488. [CrossRef]
34. Bleu, Y.; Bourquard, F.; Tite, T.; Loir, A.-S.; Maddi, C.; Donnet, C.; Garrelie, F. Review of Graphene Growth from a Solid Carbon Source by Pulsed Laser Deposition (PLD). *Front. Chem.* **2018**, *6*, 572. [CrossRef]
35. Lu, Y.; Huang, G.; Wang, S.; Mi, C.; Wei, S.; Tian, F.; Li, W.; Cao, H.; Cheng, Y. A review on diamond-like carbon films grown by pulsed laser deposition. *Appl. Surf. Sci.* **2021**, *541*, 148573. [CrossRef]
36. Casari, C.S.; Tommasini, M.; Tykwinski, R.R.; Milani, A. Carbon-atom wires: 1-D systems with tunable properties. *Nanoscale* **2016**, *8*, 4414–4435. [CrossRef]
37. Radziemski, L.J.; Cremers, D.A. (Eds.) *Laser-Induced Plasma and Applications*; Marcel Dekker: New York, NY, USA, 1989.
38. Phipps, C. (Ed.) *Laser Ablation and Its Applications*; Springer: Berlin/Heidelberg, Germany, 2007.
39. Wen, S.B.; Mao, X.; Greif, R.; Russo, R.E. Laser ablation induced vapor plume expansion into a background gas. I. Analysis. *J. Appl. Phys.* **2007**, *101*, 023114. [CrossRef]
40. Wen, S.B.; Mao, X.; Greif, R.; Russo, R.E. Laser ablation induced vapor plume expansion into a background gas. II. Experimental analysis. *J. Appl. Phys.* **2007**, *101*, 023115. [CrossRef]
41. Arnold, N.; Gruber, J.; Heitz, J. Spherical expansion of the vapor plume into ambient gas: An analytical model. *Appl. Phys. A* **1999**, *69*, S87–S93. [CrossRef]
42. Aragón, C.; Aguilera, J.A. Characterization of laser induced plasmas by optical emission spectroscopy: A review of experiments and methods. *Spectrochim. Acta B* **2008**, *63*, 893–916. [CrossRef]
43. Hahn, D.W.; Omenetto, N. Laser-Induced Breakdown Spectroscopy (LIBS), Part I: Review of Basic Diagnostics and Plasma–Particle Interactions: Still-Challenging Issues within the Analytical Plasma Community. *Appl. Spectrosc.* **2010**, *64*, 335A–366A. [CrossRef]
44. Hahn, D.W.; Omenetto, N. Laser-induced breakdown spectroscopy (LIBS), part II: Review of instrumental and methodological approaches to material analysis and applications to different fields. *Appl. Spectrosc.* **2012**, *66*, 347–419. [CrossRef]
45. Gaudiuso, R.; Dell'Aglio, M.; De Pascale, O.; Senesi, G.S.; De Giacomo, A. Laser Induced Plasma Spectroscopy for elemental analysis in environmental, cultural heritage and space applications: A review of methods and results. *Sensors* **2010**, *10*, 7434. [CrossRef]
46. Musazzi, S.; Perrini, U. *Laser-Induced Breakdown Spectroscopy: Theory and Applications*; Springer Series in Optical Sciences; Springer: Berlin/Heidelberg, Germany, 2014; Volume 182.
47. Gaudiuso, R.; Melikechi, N.; Abdel-Salam, Z.A.; Harith, M.A.; Palleschi, V.; Motto-Ros, V.; Busser, B. Laser-induced breakdown spectroscopy for human and animal health: A review. *Spectrochim. Acta B* **2019**, *152*, 123–148. [CrossRef]
48. Jantzi, S.C.; Motto-Ros, V.; Trichard, F.; Markushin, Y.; Melikechi, N.; DeGiacomo, A. Sample Treatment and Preparation for Laser-Induced Breakdown Spectroscopy. *Spectrochim. Acta B* **2016**, *115*, 52–63. [CrossRef]
49. Wang, Z.; Afgan, M.S.; Gu, W.; Song, Y.; Wang, Y.; Hou, Z.; Song, W.; Li, Z. Recent advances in laser-induced breakdown spectroscopy quantification: From fundamental understanding to data processing. *Trends Anal. Chem.* **2021**, *143*, 116385. [CrossRef]
50. Singh, J.P.; Thakur, S.N. *Laser-Induced Breakdown Spectroscopy*, 2nd ed.; Elsevier: Amsterdam, The Netherlands, 2020.
51. De Giacomo, A.; Dell'Aglio, M.; Gaudiuso, R.; Amoruso, S.; De Pascale, O. Effects of the background environment on formation, evolution and emission spectra of laser-induced plasmas. *Spectrochim. Acta B* **2012**, *78*, 1. [CrossRef]
52. Effenberger, A.J., Jr.; Scott, J.R. Effect of Atmospheric Conditions on LIBS Spectra. *Sensors* **2010**, *10*, 4907–4925. [CrossRef] [PubMed]
53. Yogesh, G.K.; Shukla, S.; Sastikumar, D.; Koinkar, P. Progress in pulsed laser ablation in liquid (PLAL) technique for the synthesis of carbon nanomaterials: A review. *Appl. Phys. A* **2021**, *127*, 810. [CrossRef]
54. De Giacomo, A.; De Bonis, A.; Dell'Aglio, M.; De Pascale, O.; Gaudiuso, R.; Orlando, S.; Santagata, A.; Senesi, G.S.; Taccogna, F.; Teghil, R. Laser Ablation of Graphite in water in a range of pressure from 1 to 146 atm using single and double pulse techniques for the production of carbon nanostructures. *J. Phys. Chem. C* **2011**, *115*, 5123. [CrossRef]
55. Santagata, A.; De Bonis, A.; De Giacomo, A.; Dell'Aglio, M.; Laurita, A.; Senesi, G.S.; Gaudiuso, R.; Orlando, S.; Teghil, R.; Parisi, G. Carbon-Based Nanostructures Obtained in Water by Ultrashort Laser Pulses. *J. Phys. Chem. C* **2011**, *115*, 5160. [CrossRef]
56. Russo, P.; Hu, A.; Compagnini, G.; Duley, W.W.; Zhou, N.Y. Femtosecond laser ablation of highly oriented pyrolytic graphite: A green route for large-scale production of porous graphene and graphene quantum dots. *Nanoscale* **2014**, *6*, 2381–2389. [CrossRef] [PubMed]
57. Compagnini, G.; Mita, V.; Cataliotti, R.S.; Puglisi, O. Short polyyne chains produced by pulsed laser ablation of graphite in water. *Carbon* **2007**, *45*, 2456–2458. [CrossRef]
58. Yang, G.W. Laser ablation in liquids: Applications in the synthesis of nanocrystals. *Prog. Mater. Sci.* **2007**, *52*, 648–698. [CrossRef]

59. Dell'Aglio, M.; Gaudiuso, R.; De Pascale, O.; De Giacomo, A. Mechanisms and processes of pulsed laser ablation in liquids during nanoparticle production. *Appl. Surf. Sci.* **2015**, *348*, 4–9. [CrossRef]
60. Fazio, E.; Gökce, B.; De Giacomo, A.; Meneghetti, M.; Compagnini, G.; Tommasini, M.; Waag, F.; Lucotti, A.; Zanchi, C.G.; Ossi, P.M.; et al. Nanoparticles Engineering by Pulsed Laser Ablation in Liquids: Concepts and Applications. *Nanomaterials* **2020**, *10*, 2317. [CrossRef] [PubMed]
61. De Giacomo, A.; Shakhatov, V.A.; Senesi, G.S.; Orlando, S. Spectroscopic investigation of the technique of plasma assisted pulsed laser deposition of titanium dioxide. *Spectrochim. Acta B* **2001**, *56*, 1459–1472. [CrossRef]
62. De Giacomo, A.; Shakhatov, V.A.; Senesi, G.S.; De Pascale, O.; Prudenzano, F. Plasma-assisted pulsed laser deposition for the improvement of the film growth process. *Appl. Surf. Sci.* **2002**, *186*, 533–537. [CrossRef]
63. Robertson, J. Diamond-like amorphous carbon. *Mater. Sci. Eng.* **2002**, *R37*, 129–281.
64. Robertson, J. Diamond-like carbon. *Pure Appl. Chem.* **1994**, *66*, 1789–1796. [CrossRef]
65. Niemczyk, A.; Moszynski, D.; Goszczyńska, A.; Kwiatkowska, M.; Jedrzejczak, A.; Nowak, D.; Sośnicki, J.G.; El Fray, M.; Baranowska, J. Understanding the DLC film—Polyamide 12 substrate interrelation during pulsed laser deposition. *Appl. Surf. Sci.* **2022**, *576 Part B*, 151872. [CrossRef]
66. Yoshida, S.; Okoshi, M.; Inoue, N. Femtosecond-pulsed laser deposition of diamond-like carbon films onto silicone rubber. *J. Phys. Conf. Ser.* **2007**, *59*, 368. [CrossRef]
67. Lackner, J.M.; Waldhauser, W.; Major, R.; Major, B.; Czarnowska, E.; Bruckert, F. Industrially scaled pulsed laser deposition based coating techniques for the realization of hemocompatible surfaces for blood contact applications. In *High-Power Laser Ablation VII*; SPIE: Cergy, France, 2008; Volume 7005, p. 70050Q.
68. Cesaria, M.; Serra, A.; Manno, D.; Rizwan Aziz, M.; Rella, S.; Malitesta, C.; Martino, M.; Verwilligen, P.; Caricato, A.P. Tailoring sheet resistance through laser fluence and study of the critical impact of a V-shaped plasma plume on the properties of PLD-deposited DLC films for micro-pattern gaseous detector applications. *Diam. Relat. Mater.* **2022**, *124*, 108909. [CrossRef]
69. Ursu, C.; Nica, P.; Rusu, B.G.; Focsa, C. V-shape plasma generated by excimer laser ablation of graphite in argon: Spectroscopic investigations. *Spectrochim. Acta B* **2020**, *163*, 105743. [CrossRef]
70. Patsalas, P.; Kaziannis, S.; Kosmidis, C.; Papadimitriou, D.; Abadias, G.; Evangelakis, G.A. Optimized pulsed laser deposition by wavelength and static electric field control: The case of tetrahedral amorphous carbon films. *J. Appl. Phys.* **2007**, *101*, 15–18. [CrossRef]
71. Xu, W.; Lin, S.; Dai, M.; Shi, Q.; Wei, C.; Zhang, X.; Zhou, K. Effects of bias voltage on the microstructure and properties of Al-doped hydrogenated amorphous carbon films synthesized by a hybrid deposition technique. *Vacuum* **2018**, *154*, 159–166. [CrossRef]
72. Zemek, J.; Houdkova, J.; Jiricek, P.; Jelinek, M. Surface and in-depth distribution of sp2 and sp3 coordinated carbon atoms in diamond-like carbon films modified by argon ion beam bombardment during growth. *Carbon* **2018**, *134*, 71–79. [CrossRef]
73. Jelinek, M.; Voss, A.; Kocourek, T.; Mozafari, M.; Vymetalova, V.; Zezulova, M.; Pisaik, P.; Kotzianova, A.; Popov, C.; Miksovsky, J. Comparison of the surface properties of DLC and ultrananocrystalline diamond films with respect to their bio-applications. *Phys. Status Solidi A* **2013**, *210*, 2106–2110. [CrossRef]
74. Jelínek, M.; Písařík, P.; Kocourek, T.; Zemek, J.; Lukeš, J. Influence of ion bombardment on growth and properties of PLD created DLC films. *Appl. Phys. A* **2013**, *110*, 943–947. [CrossRef]
75. Kocourek, T.; Jelínek, M.; Písařík, P.; Remsa, J.; Janovská, M.; Landa, M.; Zemek, J.; Havránek, V. Diamond-like carbon layers modified by ion bombardment during growth and researched by Resonant Ultrasound Spectroscopy. *Appl. Surf. Sci.* **2017**, *417*, 213–217. [CrossRef]
76. Lu, Y.; Cheng, Y.; Huang, G.; Xi, L.; Wang, S.; Wei, S.; Mi, C. Effects of external magnetic field on the micro-structure of diamondlike carbon film prepared by pulsed laser deposition. *Mater. Res. Express* **2019**, *6*, 116433. [CrossRef]
77. Modabberasl, A.; Kameli, P.; Ranjbar, M.; Salamati, H.; Ashiri, R. Fabrication of DLC thin films with improved diamond-like carbon character by the application of external magnetic field. *Carbon* **2015**, *94*, 485–493. [CrossRef]
78. Garrelie, F.; Bourquard, F.; Loir, A.-S.; Donnet, C.; Colombier, J.-P. Control of femtosecond pulsed laser ablation and deposition by temporal pulse shaping. *Opt. Laser Technol.* **2016**, *78*, 42–51. [CrossRef]
79. Jegenyes, N.; Toth, Z.; Hopp, B.; Klebniczki, J.; Bor, Z.; Fotakis, C. Femtosecond pulsed laser deposition of diamond-like carbon films: The effect of double laser pulses. *Appl. Surf. Sci.* **2006**, *252*, 4667–4671. [CrossRef]
80. Jelinek, M.; Zemek, J.; Remsa, J.; Miksovsky, J.; Kocourek, T.; Pisarik, P.; Travnickova, M.; Filova, E.; Bacakova, L. Hybrid laser technology and doped biomaterials. *Appl. Surf. Sci.* **2017**, *417*, 73–83. [CrossRef]
81. Constantinou, M.; Pervolaraki, M.; Nikolaou, P.; Prouskas, C.; Patsalas, P.; Kelires, P.; Giapintzakis, J.; Constantinides, G. Microstructure and nanomechanical properties of pulsed excimer laser deposited DLC: Ag films: Enhanced nanotribological response. *Surf. Coat. Technol.* **2017**, *309*, 320–330. [CrossRef]
82. Pisarik, P.; Jelinek, M.; Remsa, J.; Mikšovsky, J.; Zemek, J.; Jurek, K.; Kubinova, S.; Lukes, J.; Sepitka, J. Antibacterial, mechanical and surface properties of Ag-DLC films prepared by dual PLD for medical applications. *Mater. Sci. Eng. C* **2017**, *77*, 955–962. [CrossRef] [PubMed]
83. Foong, Y.M.; Koh, A.T.T.; Chua, D.H.C. Experimental and theoretical study on the energy-dependent surface evolution and microstructure changes in copper nanostructured composites. *J. Phys. D Appl. Phys.* **2011**, *44*, 385401. [CrossRef]

84. Constantinou, M.; Pervolaraki, M.; Koutsokeras, L.; Prouskas, C.; Patsalas, P.; Kelires, P.; Giapintzakis, J.; Constantinides, G. Enhancing the nanoscratch resistance of pulsed laser deposited DLC films through molybdenum-doping. *Surf. Coat. Technol.* **2017**, *330*, 185–195. [CrossRef]
85. Jelinek, M.; Kocourek, T.; Zemek, J.; Miksovsky, J.; Kubinova, S.; Remsa, J.; Kopecek, J.; Jurek, K. Chromium-doped DLC for implants prepared by laser-magnetron deposition. *Mater. Sci. Eng. C* **2015**, *46*, 381–386. [CrossRef]
86. Jelinek, M.; Zemek, J.; Vandrovcova, M.; Bacakova, L.; Kocourek, T.; Remsa, J.; Pisarik, P. Bonding and bio-properties of hybrid laser/magnetron Cr-enriched DLC layers. *Mater. Sci. Eng. C* **2016**, *58*, 1217–1224. [CrossRef] [PubMed]
87. Kumar, I.; Khare, A. Optical nonlinearity in nanostructured carbon thin films fabricated by pulsed laser deposition technique. *Thin Solid Films* **2016**, *611*, 56–61. [CrossRef]
88. Rau, J.V.; Teghil, R.; De Bonis, A.; Generosi, A.; Paci, B.; Generosi, R.; Fosca, M.; Ferro, D.; Rossi Albertini, V.; Chilingarov, N.S. Pulsed laser deposition of hard and superhard carbon thin films from C60 targets. *Diam. Relat. Mater.* **2010**, *19*, 7–14. [CrossRef]
89. Modabber Asl, A.; Kameli, P.; Ranjbar, M.; Salamati, H.; Jannesari, M. Correlations between microstructure and hydrophobicity properties of pulsed laser deposited diamond-like carbon films. *Superlatt. Microstruct.* **2015**, *81*, 64–79. [CrossRef]
90. Salah, N.; Alshahrie, A.; Iqbal, J.; Hasan, P.M.Z.; Abdel-Wahab, M.S. Tribological behavior of diamond-like carbon thin films deposited by the pulse laser technique at different substrate temperatures. *Tribol. Int.* **2016**, *103*, 274–280. [CrossRef]
91. De Bonis, A.; Rau, J.V.; Santagata, A.; Teghil, R. Diamond-like carbon thin films produced by femtosecond pulsed laser deposition of fullerite. *Surf. Coat. Technol.* **2011**, *205*, 3747–3753. [CrossRef]
92. Alawajji, R.A.; Kannarpady, G.K.; Nima, Z.A.; Kelly, N.; Watanabe, F.; Biris, A.S. Electrical properties of multilayer (DLC-TiC) films produced by pulsed laser deposition. *Appl. Surf. Sci.* **2018**, *437*, 429–440. [CrossRef]
93. Hara, T.; Yoshitake, T.; Fukugawa, T.; yun Zhu, L.; Itakura, M.; Kuwano, N.; Tomokiyo, Y.; Nagayama, K. Nanocrystalline diamond film prepared by pulsed laser deposition in a hydrogen atmosphere. *Diam. Relat. Mater.* **2004**, *13*, 679–683. [CrossRef]
94. Dementjev, A.P.; Petukhov, M.N. The roles of H and O atoms in diamond growth. *Diam. Relat. Mater.* **1997**, *6*, 486. [CrossRef]
95. Budai, J.; Toth, S.; Toth, Z.; Koos, M. Diamond-like carbon films prepared by reactive pulsed laser deposition in hydrogen and methane ambient. *Appl. Surf. Sci.* **2007**, *253*, 8220–8225. [CrossRef]
96. Ohmagari, S.; Yoshitake, T.; Nagano, A.; Al-Riyami, S.; Ohtani, R.; Setoyama, H.; Kobayashi, E.; Nagayama, K. Near-edge X-ray absorption fine structure of ultrananocrystalline diamond/hydrogenated amorphous carbon films prepared by pulsed laser deposition. *J. Nanomater.* **2009**, *2009*, 876561. [CrossRef]
97. Nagano, A.; Yoshitake, T.; Hara, T.; Nagayama, K. Optical properties of ultrananocrystalline diamond/amorphous carbon composite films prepared by pulsed laser deposition. *Diam. Relat. Mater.* **2008**, *17*, 1199–1202. [CrossRef]
98. Yoshitake, T.; Nagano, A.; Itakura, M.; Kuwano, N.; Hara, T.; Nagayama, K. Spectral absorption properties of ultrananocrystalline diamond/amorphous carbon composite thin films prepared by pulsed laser deposition. *Jpn. J. Appl. Phys.* **2007**, *46*, L936–L938. [CrossRef]
99. Yoshimoto, M.; Yoshida, K.; Maruta, H.; Hishitani, Y.; Koinuma, H.; Nishio, S.; Kakihana, M.; Tachibana, T. Epitaxial diamond growth on sapphire in an oxidizing environment. *Nature* **1999**, *399*, 340–342. [CrossRef]
100. Yoshimoto, M.; Furusawa, M.; Nakajima, K.; Takakura, M.; Hishitani, Y. Diamond film growth in an oxygen atmosphere. *Diam. Relat. Mater.* **2001**, *10*, 295–299. [CrossRef]
101. Chen, Z.Y.; Zhao, J.P.; Yano, T.; Ooie, T.; Yoneda, M.; Sakakibara, J. Growth of nano-crystalline diamond by pulsed laser deposition in oxygen atmosphere. *J. Cryst. Growth* **2001**, *226*, 62–66. [CrossRef]
102. Yoshitake, T.; Hara, T.; Nagayama, K. The influence of the repetition rate of laser pulses on the growth of diamond thin films by pulsed laser ablation of graphite. *Diam. Relat. Mater.* **2003**, *12*, 306–309. [CrossRef]
103. Yoshitake, T.; Nishiyama, T.; Nagayama, K. The role of hydrogen and oxygen gas in the growth of carbon thin films by pulsed laser deposition. *Diam. Relat. Mater.* **2000**, *9*, 689–692. [CrossRef]
104. Hara, T.; Yoshitake, T.; Fukugawa, T.; yun Zhu, L.; Itakura, M.; Kuwano, N.; Tomokiyo, Y.; Nagayama, K. Consideration of diamond film growth on various orientation substrates of diamond in oxygen and hydrogen atmospheres by reactive pulsed laser deposition. *Diam. Relat. Mater.* **2004**, *13*, 622–626. [CrossRef]
105. Hara, T.; Yoshitake, T.; Fukugawa, T.; Kubo, H.; Itakura, M.; Kuwano, N.; Tomokiyo, Y.; Nagayama, K. Ultrananocrystalline diamond prepared by pulsed laser deposition. *Diam. Relat. Mater.* **2006**, *15*, 649–653. [CrossRef]
106. Lackner, J.M.; Stotter, C.; Waldhauser, W.; Ebner, R.; Lenz, W.; Beutl, M. Pulsed laser deposition of diamond-like carbon coatings for industrial tribological applications. *Surf. Coat. Technol.* **2003**, *174–175*, 402–407. [CrossRef]
107. Popescu, A.C.; Stan, G.E.; Duta, L.; Nita, C.; Popescu, C.; Surdu, V.-A.; Husanu, M.-A.; Bita, B.; Ghisleni, R.; Himcinschi, C.; et al. The Role of Ambient Gas and Pressure on the Structuring of Hard Diamond-Like Carbon Films Synthesized by Pulsed Laser Deposition. *Materials* **2015**, *8*, 3284–3305. [CrossRef]
108. Nakazawa, H.; Osozawa, R.; Mohnai, Y.; Nara, Y. Synthesis of boron/nitrogen-incorporated diamond-like carbon films by pulsed laser deposition using nitrogen gas and a boron-containing graphite target. *Jpn. J. Appl. Phys.* **2017**, *56*, 105501. [CrossRef]
109. Al-Riyami, S.; Gima, H.; Akamine, H.; Yoshitake, T. Chemical bonding of nitrogenated ultrananocrystalline diamond films deposited on titanium substrates by pulsed laser deposition. *ECS J. Solid State Sci. Technol.* **2013**, *2*, M33–M38. [CrossRef]
110. Ray, S.C.; Mbiombi, W.; Papakonstantinou, P. Electrical and electronic properties of nitrogen doped amorphous carbon (a-CNx) thin films. *Curr. Appl. Phys.* **2014**, *14*, 1845–1848. [CrossRef]

111. Ray, S.C.; Pong, W.F.; Papakonstantinou, P. Iron, nitrogen and silicon doped diamond like carbon (DLC) thin films: A comparative study. *Thin Solid Films* **2016**, *610*, 42–47. [CrossRef]
112. Menegazzo, N.; Kahn, M.; Berghauser, R.; Waldhauser, W.; Mizaikoff, B. Nitrogen-doped diamond-like carbon as optically transparent electrode for infrared attenuated total reflection spectroelectrochemistry. *Analyst* **2011**, *136*, 1831–1839. [CrossRef]
113. Guzman, F.; Favre, M.; Ruiz, H.M.; Hevia, S.; Caballero, L.S.; Wyndham, E.S.; Bhuyan, H.; Flores, M.; Mandl, S. Pulsed laser deposition of thin carbon films in a neutral gas background. *J. Phys. D Appl. Phys.* **2013**, *46*, 215202. [CrossRef]
114. Ossi, P.M.; Bottani, C.E.; Miotello, A. Pulsed-laser deposition of carbon: From DLC to cluster-assembled films. *Thin Solid Films* **2005**, *482*, 2–8. [CrossRef]
115. Gaudiuso, R. Experimental Techniques for the Study of Laser Induced Plasmas and Their Applications to Chemical Analysis and Materials Production. Ph.D. Thesis, University of Bari "A. Moro", Bari, Italy, 2010.
116. Ferrari, A.C.; Robertson, J. Interpretation of Raman spectra of disordered and amorphous carbon. *Phys. Rev. B* **2000**, *61*, 14095–14107. [CrossRef]
117. Novoselov, K.S.; Geim, A.K.; Morozov, S.V.; Jiang, D.; Zhang, Y.; Dubonos, S.V.; Grigorieva, I.V.; Firsov, A.A. Electric field effect in atomically thin carbon films. *Science* **2004**, *306*, 666–669. [CrossRef]
118. Geim, A.K. Graphene: Status and prospects. *Science* **2009**, *324*, 1530–1534. [CrossRef] [PubMed]
119. Urade, A.R.; Lahiri, I.; Suresh, K.S. Graphene Properties, Synthesis and Applications: A Review. *JOM* **2023**, *75*, 614–630. [CrossRef] [PubMed]
120. Ghany, N.A.A.; Elsherif, S.A.; Handal, H.T. Revolution of Graphene for different applications: State-of-the-art. *Surf. Interfaces* **2017**, *9*, 93–106. [CrossRef]
121. Cappelli, E.; Iacobucci, S.; Scilletta, C.; Flammini, R.; Orlando, S.; Mattei, G.; Ascarelli, P.; Borgatti, F.; Giglia, A.; Mahn, N.; et al. Orientation tendency of PLD carbon films as a function of substrate temperature: A NEXAFS. study. *Diam. Relat. Mater.* **2005**, *14*, 959–964. [CrossRef]
122. Cappelli, E.; Orlando, S.; Servidori, M.; Scilletta, C. Nano-graphene structures deposited by N-IR pulsed laser ablation of graphite on Si. *Appl. Surf. Sci.* **2007**, *254*, 1273–1278. [CrossRef]
123. Benhagouga, R.H.; Abdelli-Messaci, S.; Abdesselam, M.; Blondeau-Patissier, V.; Yahiaoui, R.; Siad, M.; Rahal, A. Temperature effect on hydrogenated amorphous carbon leading to hydrogenated graphene by pulsed laser deposition. *Appl. Surf. Sci.* **2017**, *426*, 874–880. [CrossRef]
124. Ren, P.; Pu, E.; Liu, D.; Wang, Y.; Xiang, B.; Ren, X. Fabrication of nitrogen-doped graphenes by pulsed laser deposition and improved chemical enhancement for Raman spectroscopy. *Mater. Lett.* **2017**, *204*, 65–68. [CrossRef]
125. Lopez, D.; Castellanos, M.A.; Riascos, H. Influence of substrate temperature on graphene oxide thin films synthesis by laser ablation technique. *J. Vac. Sci. Technol. A* **2022**, *40*, 013402. [CrossRef]
126. Bleu, Y.; Bourquard, F.; Gartiser, V.; Loir, A.-S.; Caja-Munoz, B.; Avila, J.; Barnier, V.; Garrelie, F.; Donnet, C. Graphene synthesis on SiO_2 using pulsed laser deposition with bilayer predominance. *Mater. Chem. Phys.* **2019**, *238*, 121905. [CrossRef]
127. Kumar, S.R.S.; Alshareef, H.N. Ultraviolet laser deposition of graphene thin films without catalytic layers. *Appl. Phys. Lett.* **2013**, *102*, 012110. [CrossRef]
128. Kumar, I.; Khare, A. Multi- and few-layer graphene on insulating substrate via pulsed laser deposition technique. *Appl. Surf. Sci.* **2014**, *317*, 1004–1009. [CrossRef]
129. Milenov, T.; Dikovska, A.; Avdeev, G.; Avramova, I.; Kirilov, K.; Karashanova, D.; Terziyska, P.; Georgieva, B.; Arnaudov, B.; Kolev, S.; et al. Pulsed laser deposition of thin carbon films on SiO_2/Si substrates. *Appl. Surf. Sci.* **2019**, *480*, 323–329. [CrossRef]
130. Xu, S.C.; Man, B.Y.; Jiang, S.; Liu, A.H.; Hu, G.; Chen, C.S.; Liu, M.; Yang, C.; Feng, D.J.; Zhang, C. Direct synthesis of graphene on any nonmetallic substrate based on KrF laser ablation of ordered pyrolytic graphite. *Laser Phys. Lett* **2014**, *11*, 096001. [CrossRef]
131. Wang, J.; Wang, X.; Yu, J.; Xiao, T.; Peng, L.; Fan, L.; Wang, C.; Shen, Q.; Wu, W. Tailoring the Grain Size of Bi-Layer Graphene by Pulsed Laser Deposition. *Nanomaterials* **2018**, *8*, 885. [CrossRef]
132. Wang, J.; Fan, L.; Wang, X.; Xiao, T.; Peng, L.; Wang, X.; Yu, J.; Cao, L.; Xiong, Z.; Fu, Y.; et al. Pulsed laser deposition of monolayer and bilayer graphene. *Appl. Surf. Sci.* **2019**, *494*, 651–658. [CrossRef]
133. Juvaid, M.M.; Sarkar, S.; Gogoi, P.K.; Ghosh, S.; Annamalai, M.; Lin, Y.-C.; Prakash, S.; Goswami, S.; Li, C.; Hooda, S.; et al. Direct Growth of Waferscale, Transparent, p-Type Reduced Graphene Oxide Like Thin Films by Pulsed Laser Deposition. *ACS Nano* **2020**, *14*, 3290–3298. [CrossRef] [PubMed]
134. Kumar, P.; Lahiri, I.I.; Mitra, A. Nickel mediated few-layer graphene growth on glass substrates by pulsed laser deposition. *Results Phys.* **2019**, *14*, 102350. [CrossRef]
135. Kumar, P.; Lahiri, I.; Mitra, A. Influence of the buffer layers on growth and quality of graphene films grown by pulsed laser deposition. *Mater. Res. Express* **2019**, *6*, 125625. [CrossRef]
136. Wang, K.; Tai, G.; Wong, K.H.; Lau, S.P.; Guo, W. Ni induced few-layer graphene growth at low temperature by pulsed laser deposition. *AIP Adv.* **2011**, *1*, 022141. [CrossRef]
137. Bourquard, F.; Bleu, Y.; Loir, A.-S.; Caja-Munoz, B.; Avila, J.; Asensio, M.-C.; Raimondi, G.; Shokouhi, M.; Rassas, I.; Farre, C.; et al. Electroanalytical Performance of Nitrogen-Doped Graphene Films Processed in One Step by Pulsed Laser Deposition Directly Coupled with Thermal Annealing. *Materials* **2019**, *12*, 666. [CrossRef]
138. Larki, F.; Kameli, P.; Nikmanesh, H.; Jafari, M.; Salamati, H. The influence of external magnetic field on the pulsed laser deposition growth of graphene on nickel substrate at room temperature. *Diam. Relat. Mater.* **2019**, *93*, 233–240. [CrossRef]

139. Bleu, Y.; Bourquard, F.; Loir, A.-S.; Barnier, V.; Garrelie, F.; Donnet, C. Raman study of the substrate influence on graphene synthesis using a solid carbon source via rapid thermal annealing. *J. Raman Spectrosc.* **2019**, *50*, 1630–1641. [CrossRef]
140. Maddi, C.; Bourquard, F.; Barnier, V.; Avila, J.; Asensio, M.C.; Tite, T.; Donnet, C.; Garrelie, F. Nano-architecture of nitrogen-doped graphene films synthesized from a solid CN source. *Sci. Rep.* **2018**, *8*, 3247. [CrossRef]
141. Tite, T.; Donnet, C.; Loir, A.-S.; Reynaud, S.; Michalon, J.-Y.; Vocanson, F.; Garrelie, F. Graphene-based textured surface by pulsed laser deposition as a robust platform for surface enhanced Raman scattering applications. *Appl. Phys. Lett.* **2014**, *104*, 041912. [CrossRef]
142. Dong, X.; Liu, S.; Song, H.; Gu, P. Growth of large-area, few-layer graphene by femtosecond pulsed laser deposition with double-layer Ni catalyst. *J. Mater. Sci.* **2017**, *52*, 2060–2065. [CrossRef]
143. Tite, T.; Barnier, V.; Donnet, C.; Loir, A. –S.; Reynaud, S.; Michalon, J.–Y.; Vocanson, F.; Garrelie, F.; Surface enhanced Raman spectroscopy platform based on graphene with one-year stability. *Thin Solid Films* **2016**, *604*, 74–80. [CrossRef]
144. Li, X.; Cai, W.; Colombo, L.; Ruoff, R.S. Evolution of Graphene Growth on Ni and Cu by Carbon Isotope Labeling. *Nano Lett.* **2009**, *9*, 4268–4272. [CrossRef] [PubMed]
145. Vishwakarma, R.; Rosmi, M.S.; Takahashi, K.; Wakamatsu, Y.; Yaakob, Y.; Araby, M.I.; Kalita, G.; Kitazawa, M.; Tanemurab, M. Transfer free graphene growth on SiO_2 substrate at 250 °C. *Sci. Rep.* **2017**, *7*, 43756. [CrossRef] [PubMed]
146. Abd Elhamid, A.M.; Aboulfotouh, A.M.; Hafez, M.A.; Azzouz, I.M. Room temperature graphene growth on complex metal matrix by PLD. *Diam. Relat. Mater.* **2017**, *80*, 162–167. [CrossRef]
147. Koh, A.T.T.; Foong, Y.M.; Chua, D.H.C. Comparison of the mechanism of low defect few-layer graphene fabricated on different metals by pulsed laser deposition. *Diam. Relat. Mater.* **2012**, *25*, 98–102. [CrossRef]
148. Maddi, C.; Bourquard, F.; Tite, T.; Loir, A.S.; Donnet, C.; Garrelie, F.; Barnier, V.; Wolski, K.; Fortgang, P.; Zehani, N.; et al. Structure, electrochemical properties and functionalization of amorphous CN films deposited by femtosecond pulsed laser ablation. *Diam. Relat. Mater.* **2016**, *65*, 17–25. [CrossRef]
149. Scilletta, C.; Servidori, M.; Orlando, S.; Cappelli, E.; Barba, L.; Ascarelli, P. Influence of substrate temperature and atmosphere on nano-graphene formation and texturing of pulsed Nd:YAG laser-deposited carbon films. *Appl. Surf. Sci.* **2006**, *252*, 4877–4881. [CrossRef]
150. Qian, M.; Zhou, Y.S.; Gao, Y.; Park, J.B.; Feng, T.; Huang, S.M.; Sun, Z.; Jiang, L.; Lu, Y.F. Formation of graphene sheets through laser exfoliation of highly ordered pyrolytic graphite. *Appl. Phys. Lett.* **2011**, *98*, 173108. [CrossRef]
151. Ershov, I.V.; Prutsakova, N.V.; Holodova, O.M.; Lavrentyev, A.A.; Mardasova, I.V.; Zhdanova, T.P. Structural Properties and Composition of Graphite-Like Carbon Films Obtained by Pulsed Laser Deposition. *Tech. Phys.* **2021**, *66*, 580–587. [CrossRef]
152. Ershov, I.V.; Lavrentyev, A.A.; Prutsakova, N.V.; Holodova, O.M.; Mardasova, I.V.; Zhdanova, T.P.; Kozakov, A.T. Characterization of Graphenic Carbon Produced by Pulsed Laser Ablation of Sacrificial Carbon Tapes. *Appl. Sci.* **2021**, *11*, 11972. [CrossRef]
153. Kumar, S.R.S.; Nayak, P.K.; Hedhili, M.N.; Khan, M.A.; Alshareef, H.N. In situ growth of p and n-type graphene thin films and diodes by pulsed laser deposition. *Appl. Phys. Lett.* **2013**, *103*, 192109. [CrossRef]
154. Ferrari, A.C.; Meyer, J.C.; Scardaci, V.; Casiraghi, C.; Lazzeri, M.; Mauri, F.; Piscanec, S.; Jiang, D.; Novoselov, K.S.; Roth, S.; et al. Raman Spectrum of Graphene and Graphene Layers. *Phys. Rev. Lett.* **2006**, *97*, 187401. [CrossRef] [PubMed]
155. Bleu, Y.; Bourquard, F.; Barnier, V.; Lefkir, Y.; Reynaud, S.; Loir, A.-S.; Garrelie, F.; Donnet, C. Boron-doped graphene synthesis by pulsed laser co-deposition of carbon and boron. *Appl. Surf. Sci.* **2020**, *513*, 145843. [CrossRef]
156. Georgakilas, V.; Otyepka, M.; Bourlinos, A.B.; Chandra, V.; Kim, N.; Kemp, K.C.; Hobza, P.; Zboril, R.; Kim, K.S. Functionalization of Graphene: Covalent and Non-Covalent Approaches, Derivatives and Applications. *Chem. Rev.* **2012**, *112*, 6156–6214. [CrossRef]
157. Plšek, J.; Drogowska-Horná, K.A.; Guerra, V.L.P.; Mikšátko, J.; Valeš, V.; Kalbáč, M. Towards Catalytically Active Porous Graphene Membranes with Pulsed Laser Deposited Ceria Nanoparticles. *Chem. Eur. J.* **2021**, *27*, 4150–4158. [CrossRef]
158. Casari, C.S.; Milani, A. Carbyne: From the elusive allotrope to stable carbon atom wires. *MRS Commun.* **2018**, *8*, 207–219. [CrossRef]
159. Hearth, J.R.; Zhang, Q.; O'Brien, S.C.; Curl, R.F.; Kroto, H.W.; Smalley, R.E. The formation of long carbon chain molecules during laser vaporization of graphite. *J. Am. Chem. Soc.* **1987**, *109*, 359–363. [CrossRef]
160. Compagnini, G.; Battiato, S.; Puglisi, O.; Baratta, G.A.; Strazzulla, G. Ion irradiation of sp rich amorphous carbon thin films: A vibrational spectroscopy investigation. *Carbon* **2005**, *43*, 3025. [CrossRef]
161. Hu, A.; Rybachuk, M.; Lu, Q.-B.; Duley, W.W. Direct synthesis of sp-bonded carbon chains on graphite surface by femtosecond laser irradiation. *Appl. Phys. Lett.* **2007**, *91*, 131906. [CrossRef]
162. Hu, A.; Lu, Q.-B.; Duley, W.W.; Rybachuk, M. Spectroscopic characterization of carbon chains in nanostructured tetrahedral carbon films synthesized by femtosecond pulsed laser deposition. *J. Chem. Phys.* **2007**, *126*, 154705. [CrossRef]
163. Casari, C.S.; Giannuzzi, C.S.; Russo, V. Carbon-atom wires produced by nanosecond pulsed laser deposition in a background gas. *Carbon* **2016**, *104*, 190–195. [CrossRef]
164. Park, Y.E.; Shin, S.K.; Park, S.M. The physical effects on the formation of polyynes by laser ablation. *Chem. Phys. Lett.* **2013**, *568–569*, 112–116. [CrossRef]
165. Pan, B.; Xiao, J.; Li, J.; Liu, P.; Wang, C.; Yang, G. Carbyne with finite length: The one-dimensional sp carbon. *Sci. Adv.* **2015**, *1*, e1500857. [CrossRef]
166. Tabata, H.; Fujii, M.; Hayashi, S. Laser ablation of diamond nanoparticles suspended in solvent: Synthesis of polyynes. *Chem. Phys. Lett.* **2004**, *395*, 138–142. [CrossRef]

167. Tabata, H.; Fujii, M.; Hayashi, S. Laser ablation of diamond particles suspended in ethanol: Effective formation of long polyynes. *Carbon* **2006**, *44*, 522–529. [CrossRef]
168. Wakabayashi, T.; Nagayama, H.; Daigoku, K.; Kiyooka, Y.; Hashimoto, K. Laser induced emission spectra of polyyne molecules $C_{2n}H_2$ (n = 5–8). *Chem. Phys. Lett.* **2007**, *446*, 65–70. [CrossRef]
169. Kucherik, A.O.; Osipov, A.V.; Arakelian, S.M.; Garnov, S.V.; Povolotckaya, A.V.; Kutrovskaya, S.V. The laser-assisted synthesis of linear carbon chains stabilized by noble metal particle. *J. Phys. Conf. Ser.* **2019**, *1164*, 012006. [CrossRef]
170. Baughman, R.H. Dangerously Seeking Linear Carbon. *Science* **2006**, *312*, 1009–1110. [CrossRef]
171. Dave, H.A.B.; Matthijn, D.; Guus, R. Pulsed laser deposition in Twente: From research tool towards industrial deposition. *J. Phys. D Appl. Phys.* **2014**, *47*, 034006.
172. Zanoni, K.P.S.; Pérez-del-Rey, D.; Dreessen, C.; Rodkey, N.; Sessolo, M.; Soltanpoor, W.; Morales-Masis, M.; Bolink, H.J. Tin(IV) Oxide Electron Transport Layer via Industrial-Scale Pulsed Laser Deposition for Planar Perovskite Solar Cells. *ACS Appl. Mater. Interfaces* **2023**, *15*, 32621–32628. [CrossRef]
173. Lackner, J.M. Industrially-scaled large-area and high-rate tribological coating by Pulsed Laser Deposition. *Surf. Coat. Technol.* **2005**, *200*, 1439–1444. [CrossRef]
174. Yao, J.D.; Zheng, Z.Q.; Yang, G.W. Production of large-area 2D materials for high-performance photodetectors by pulsed-laser deposition. *Prog. Mater. Sci.* **2019**, *106*, 100573. [CrossRef]